Mechanism of Selective Oxidation and Ammoxidation of Propene on Bismuth Molybdates from DFT Calculations on Model Clusters

Yun Hee Jang[†] and William A. Goddard III*

Materials and Process Simulation Center (139-74), California Institute of Technology, Pasadena, California 91125

Received: March 26, 2002

In this paper, we use first principles quantum mechanical methods (B3LYP flavor of Density Functional Theory) to examine the mechanism of selective oxidation and ammoxidation of propene by $BiMoO_x$ catalysts. To do this, we use finite clusters chosen to mimic likely sites on the heterogeneous surfaces of the catalysts. We conclude that activation of the propene requires a Bi(V) site, whereas all subsequent reactions involve di-oxo Mo(VI) sites adjacent to the Bi. We find that two such Mo sites are required for the most favorable reactions. These results are compatible with current experimental data. For ammoxidation, we conclude that ammonia activation would be easier on Mo(IV) rather than on Mo(VI). Ammonia would be activated more easily for more reducing condition. Because ammonia and propene are reducing agents, higher partial pressures of them could accelerate the ammonia activation. This is consistent with the kinetic model of ammoxidation proposed by Grasselli and co-workers that imido sites (Mo═NH) are more abundant in higher partial pressures of feed. Our calculations also indicate that allyl groups produced as a result of the hydrogen abstraction from propenes would be adsorbed more easily on imido groups (Mo═NH) than on oxo groups (Mo═O) and that the spectator oxo effect is larger than spectator imido effect. Thus, we propose that the best site for ammoxidation (at least for allyl adsorption) is the imido group of the "oxo-imido" species.

1. Introduction

Despite the keen industrial interest in selective oxidation and ammoxidation of small alkanes (CH_4, C_2H_6, C_3H_8, and C_4H_{10}) by mixed metal oxides, there is little in the way of definitive mechanism known for the most effective catalysts. To learn more about the reaction mechanism of these important catalysts, we are using a variety of first principles theoretical approaches to calculate the fundamental steps.

As the first step, we examined the selective oxidation and ammoxidation of propene[1,2] for which there are some experimental data relating to mechanism

$$CH_3CHCH_2(\text{propene}) + O_2 \xrightarrow{300-450\ ^\circ C} CH_2CHCHO\ (\text{acrolein}) + H_2O \quad (1)$$

$$CH_3CHCH_2(\text{propene}) + NH_3 + \frac{3}{2}O_2 \xrightarrow{400-460\ ^\circ C} CH_2CHCN\ (\text{acrylonitrile}) + 3H_2O \quad (2)$$

One of the most active and selective catalysts for these reactions is based on bismuth molybdate.[2−4] The mechanism has been proposed as follows:[5,6]

(1) Allylic H abstraction at a bismuth site resulting in an allyl intermediate adsorbing on a molybdenum site (rate-determining step),

(2) O insertion into the allyl intermediate at the molybdenum site and abstraction of a second H,

(3) Elimination of the H_2O to remove the H from the bismuth oxide, and

(4) Reoxidation of the Bi and Mo sites.

The "dual-site" concept is widely accepted, where the bismuth site is responsible for the C−H activation and the molybdenum site is responsible for allyl adsorption and oxygen insertion. Ammoxidation proceeds essentially in the same way as oxidation, except that (1) ammonia is first activated on molybdenum site to create imido groups (═NH) from oxo groups (═O) and (2) NH rather than O is inserted into the allyl group.

In this study, we investigated this reaction path on the model clusters of the component oxides (Bi_2O_3 and MoO_3) using ab initio quantum-mechanical (QM) methods (DFT-B3LYP). The same reactions had been investigated theoretically in 1980s.[7] Calculation methods and computers have been dramatically improved since then, and our work is reexamining the reaction with more advanced methods and fewer simplications. This work could also be a theoretical background to a current catalyst development with a greater opportunity—ammoxidation catalysts operating on propane rather than propene.

2. Calculation Details

2.1. Model Clusters. A schematic representation of the crystal structures of the component oxides of bismuth molybdate, α-MoO_3 and α-Bi_2O_3, are given in Figure 1. In α-MoO_3,[8] each molybdenum site consists of a tetrahedron with two terminal oxo oxygens [r(Mo═O) ≈ 1.7 Å] and two bridging oxygens [r(Mo−O) ≈ 1.9 Å] connected to a molybdenum atom in its nearest-neighbor coordination shell. In α-Bi_2O_3,[9] each bismuth has three nearest-neighbor oxygens connected to it and one lone pair. Similar bonding configuration can be found in one of the bismuth molybdate, α-$Bi_2Mo_3O_{12}$,[10,11] as shown in Figure 1c.

* To whom correspondence should be addressed. E-mail: wag@wag.caltech.edu.

† Current address: School of Chemistry, Seoul National University, Seoul 151-747, Korea.

10.1021/jp0208081 CCC: $22.00
Published on Web 05/18/2002

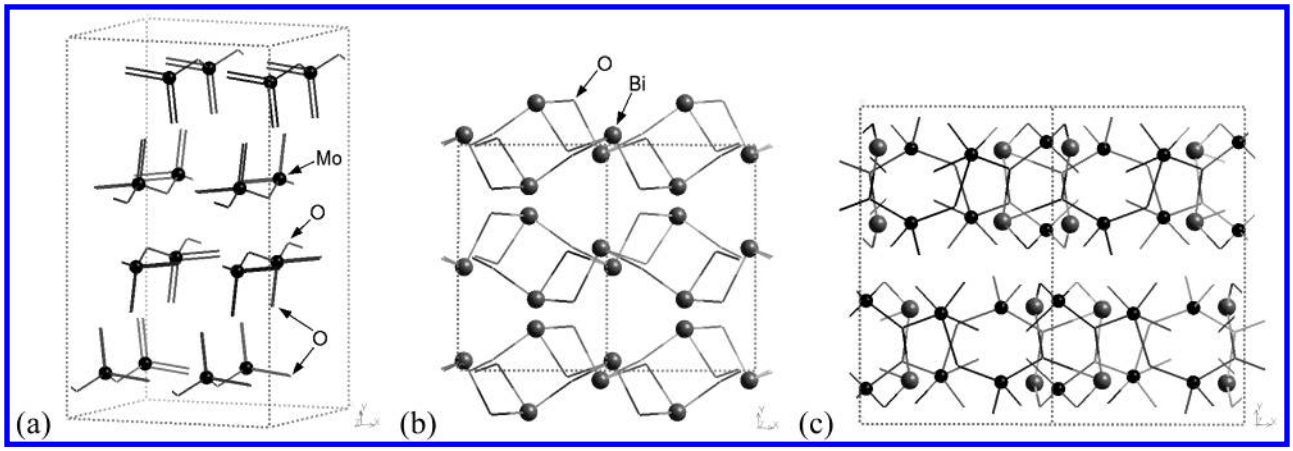

Figure 1. Crystal structures of the component oxides of bismuth molybdate. (a) $2 \times 1 \times 2$ cell of α-MoO_3[8] and (b) $2 \times 1 \times 1$ cell of α-Bi_2O_3.[9] (c) Crystal structure of one of phases of bismuth molybdate, a $2 \times 1 \times 2$ cell of α-$Bi_2Mo_3O_{12}$.[10,11] Black balls represent Bi, gray balls represent Mo, and the rest of atoms are oxygens.

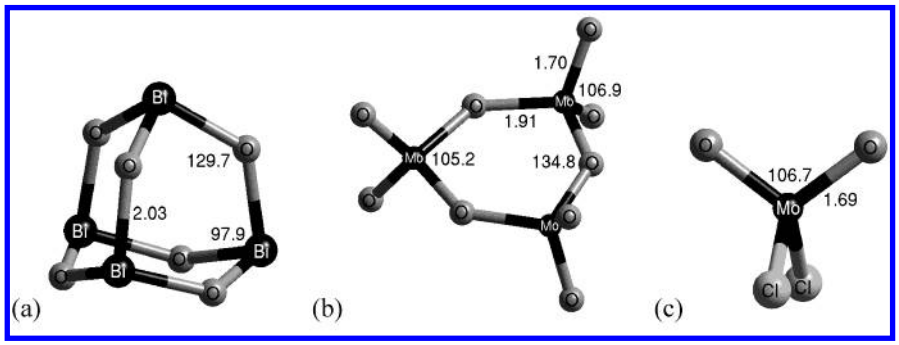

Figure 2. Model clusters used to represent (a) the bismuth site (Bi_4O_6) and (b) the molybdenum site (Mo_3O_9). (c) Smaller model cluster used to represent the molybdenum site instead of (b) in the later part of the work. Selected geometrical parameters (bond lengths and angles) are shown together in Å and in degrees, respectively.

To represent each site, we chose the model clusters having the same stoichiometry and connectivity as in the crystal structure. The Bi_4O_6 cluster (Figure 2a) has three oxygens connected to each bismuth atom, and the Mo_3O_9 cluster (Figure 2b) has two terminal oxo oxygens and two bridging oxygens connected to each molybdenum atom.

The Mo_3O_9 cluster has been found to be one of the most abundant gas-phase molybdenum oxide cluster species (cations and anions) generated from the evaporation of the MoO_3 oxide samples from an effusion source (Knudsen cell).[12−14] Its six-ring structure has been suggested as the lowest-energy structure.[12,14] The Bi_4O_6 cluster in the adamantane-type cage structure has been proposed as a neutral species present in the gas phase,[15−18] and the cationic species $Bi_4O_6^+$ has been recently detected from the laser vaporization experiment from a bismuth rod with an expansion gas seeded with oxygen.[19] There have been many recent experiments on the reaction of these mass-selected gas-phase metal oxide clusters with small molecules such as ammonia, ethene, and propene as a model study of the heterogeneous catalysis.[14,19−21] Consequently, our calculations employing these model clusters should help interpret the experimental results.

Our studies find that the terminal oxo oxygens lead to reactions on the Mo site that are far more favorable than for the bridging oxygens (see the section 3.1). Appendix A compares the energetics for several key processes with the Mo_3O_9 cluster with the results on the smaller MoO_2Cl_2 cluster (Figure 2c) in which the bridging oxygen atoms are replaced with chlorine atoms. We find essentially identical energetics. Consequently, most of our studies on the mechanism used the smaller MoO_2Cl_2 cluster.

2.2. Calculational Methods. *2.2.1. Quantum Mechanics.* We used the B3LYP flavor of density-functional theory (DFT) which includes the generalized gradient approximation and a component of the exact Hartree−Fock (HF) exchange.[22−26] The Dunning cc-pVTZ(-f) basis set[27,28] was used for H, C, N, and O. The effective core potentials (ECP) and basis set of Hay and Wadt were used for Mo and Bi [LACVP**].[29] The 6-31G** basis set was used for chlorines (Cl) replacing bridging oxygens. All the calculations were carried out using Jaguar 3.5[30,31] and in the restricted open-shell DFT (RODFT) (except as noted).

2.2.2. Energetics. For each structure, the geometry was fully optimized and shown to be a minimum. Vibration frequencies were calculated from the Hessian (second derivative matrix) and used to obtain zero-point energies (ZPE) and thermodynamic properties (enthalpy and free energy) at the reaction temperature of 673 K as in (1) and (2) or at room-temperature (298 K)

$$\Delta G_{673} = E + \mathrm{ZPE} + \Delta\Delta G_{0\rightarrow 673} \qquad (3)$$

The dissociation energies (enthalpies) at 298 K, D_{298}, of several relevant molecules are given in Table 1, indicating good agreement between calculation and experiment. For the B3LYP case both RODFT and UDFT calculations give similar results. Consequently, we use RODFT/B3LYP for the other calculations in this paper.

3. Oxidation

3.1. First Step: H-Abstraction. The calculated C−H bond strengths of propene are listed in Table 2. As expected the C_α−H_α bond is weakest, leading to $D_{298} = 86.8$ kcal/mol in excellent agreement with the experimental value of 86.5 ± 2.1 kcal/mol.

TABLE 1: Dissociation Energies D_{298} (kcal/mol) of Relevant Molecules Calculated at 298 K with the B3LYP Flavor of Restricted Open-Shell Density-Functional Theory (RODFT)

	RODFT	UDFT[g]			experiment[a]	
	B3LYP	B3LYP	BLYP	PW91		
H−CH_3	104.6	103.6	102.9	103.4	104.9 ± 0.1[b]	$\Delta H(^2CH_3) + \Delta H(^2H) - \Delta H(CH_4)$
H−CH_2CHCH_2	86.8	84.4	82.9	83.7	86.5 ± 2.1[b,c]	$\Delta H(^2\text{allyl}) + \Delta H(^2H) - \Delta H(\text{propene})$
Bi−O	84.5	84.5	100.0	97.6	81 ± 3[d,e]	$\Delta H(^4Bi) + \Delta H(^3O) - \Delta H(^2BiO)$
Mo−O	113.1	113.8	133.8	131.6	134 ± 5[d],125.4 ± 0.9[f]	$\Delta H(^7Mo) + \Delta H(^3O) - \Delta H(^5MoO)$

[a] Ref 32. [b] Ref 33. [c] Ref 34. [d] Ref 35. [e] Other experimental data: 81.0 ± 1.4 kcal/mol[36] and 79.6 ± 0.7 at 0 K[18] (At 0 K, we calculate $D_0 = 83.71$ kcal/mol (B3LYP)). [f] Ref 37. [g] For comparison, the values calculated at other DFT levels (B3LYP, BLYP, and PW91 flavors of unrestricted DFT (UDFT)) are also listed. For the unrestricted DFT calculations, Jaguar v4.0 was used.

TABLE 2: C−H Bond Strengths of Propene in the Gas Phase. (a) Bond Dissociation Enthalpy D_{298} (kcal/mol) at 298 K and (b) Bond Dissociation Free Energy ΔG_{673} at 673 K during C−H Cleavage from C_3H_6 to $^2C_3H_5$ (three different bonds)

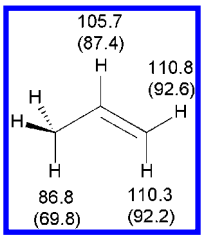

	(a) D_{298}	(b) ΔG_{673}
$C_\alpha-H_\alpha$	86.8	69.8
$C_\beta-H_\beta$	105.7	87.4
$C_\gamma-H_\gamma$	110.8	92.6

The H-abstracting ability of each site was investigated by calculating the free energy cost of the following process

$$Mo_3O_9 + \text{propene} \rightarrow Mo_3O_9H + \text{allyl} \quad (4)$$

$$Bi_4O_6 + \text{propene} \rightarrow Bi_4O_6H + \text{allyl} \quad (5)$$

where the $C_\alpha-H_\alpha$ bond of propene is cleaved to produce an allyl radical in the gas-phase and an H atom adsorbed on each site. All oxygens are equivalent in the Bi_4O_6 cluster, but there are two different types of oxygens in the Mo_3O_9 cluster, the terminal oxo oxygens and the bridging oxygens. The optimized structure of each cluster with hydrogen adsorbed on each adsorption site is shown in Figure 3, and the energy changes are listed in Table 3. The energetics for the various reaction steps to be described below are collected together in Scheme 1.

3.1.1. Mo Site. The energy cost at 673 K (ΔG_{673}) is 27.1 or 42.8 kcal/mol on molybdenum site, depending on whether the dissociated H adsorbs on the terminal oxo oxygen or on the bridging oxygen. Because the dissociation free energy of

TABLE 3: Energy Change (kcal/mol) during H-Abstraction from Propene to Each Cluster

	ΔE	ΔZPE	$\Delta\Delta G_{0\rightarrow673}$	ΔG_{673}
(a) Mo_3O_9 + propene → Mo_3O_9H (H on O_{oxo}) + allyl	32.9	−2.4	−3.4	27.1
(b) Mo_3O_9 + propene → Mo_3O_9H (H on O_{bridge}) + allyl	50.7	−2.3	−5.6	42.8
(c) Bi_4O_6 + propene → Bi_4O_6H + allyl	50.9	−1.6	−7.6	41.6

SCHEME 1: Summary of the Hydrogen Abstraction from Propene by (a) the Molybdenum Site (implausible) and (b) the Bismuth Site (plausible only on the oxidized site, which is likely consumed very quickly). Energy Changes are Presented in kcal/mol

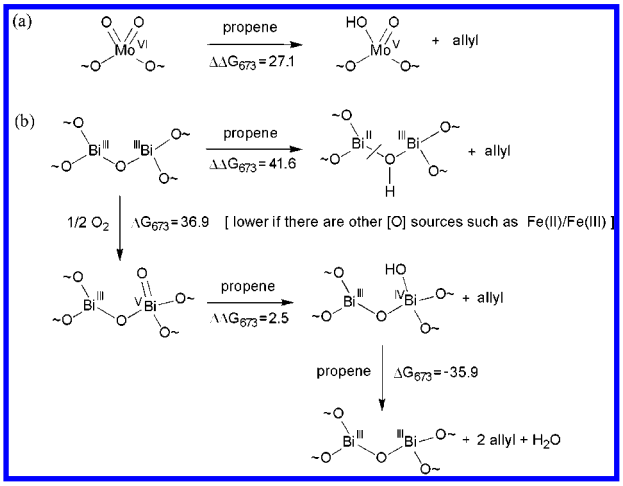

propene at 673 K is 69.8 kcal/mol, the binding free energy of hydrogen on Mo_3O_9 is estimated as 42.7 kcal/mol (exothermic) on the terminal oxygen and as 27.0 kcal/mol on the bridging oxygen. The π-bond between Mo and the terminal oxygen is 15 kcal/mol easier to activate than the bond between Mo and the bridging oxygen, so that the terminal oxygen serves as a

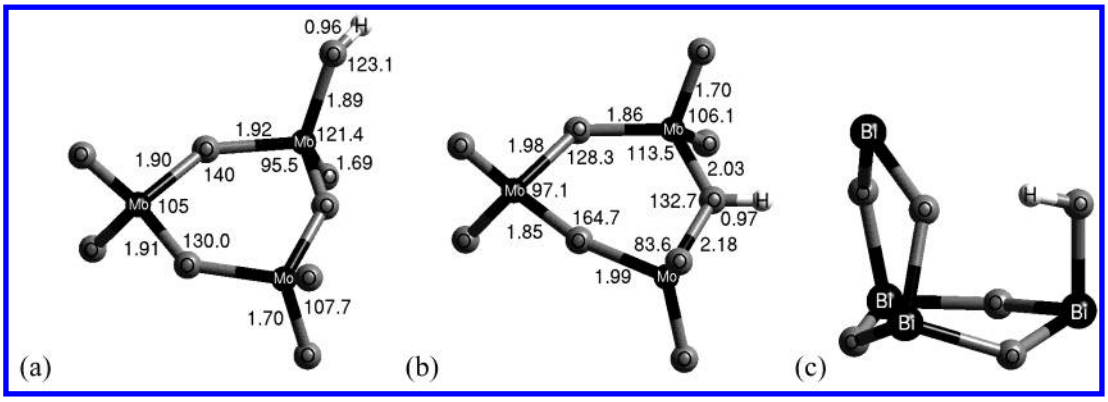

Figure 3. Optimized structures showing a hydrogen adsorbed on (a) an oxo group of Mo_3O_9, (b) a bridging oxygen of Mo_3O_9, and (c) on an oxygen of Bi_4O_6. Selected geometrical parameters (bond lengths and angles) are shown together in Å and in degrees, respectively.

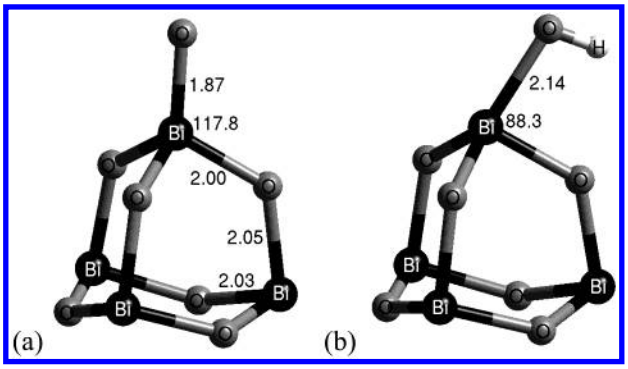

Figure 4. Optimized structures of (a) Bi_4O_7 where a Bi(III) was oxidized to Bi(V) and (b) Bi_4O_7H where one hydrogen was abstracted from propene to this oxidized Bi(V) site. Selected geometrical parameters (bond lengths and angles) are shown together in Å and in degrees, respectively.

stronger adsorption site, as proposed from other work.[38−40] However, in either case, the H abstraction by Mo_3O_9 is too endothermic to be plausible at 673 K.

3.1.2. Bi(III) Site. The corresponding energy cost is 41.6 kcal/mol on bismuth site. [The binding free energy of H this site is estimated as 28.2 kcal/mol.] This is even more endothermic than on molybdenum site (27.1 kcal/mol), probably because it leads to Bi−O bond cleavage and hence produces a very unfavorable reduced Bi(II) site. This seems contrary to the widely accepted view that the bismuth site is responsible for the C−H activation of propene.

3.1.3. Bi(V) Site. However, bismuth oxide (Bi_2O_3) is known to have a unique ability to chemisorb O_2 dissociatively. Here, Bi(III) ($5d^{10}6s^26p^0$) is oxidized to Bi(V) ($5d^{10}6s^06p^0$)[41,42] with the Bi lone pairs responsible for reducing dioxygen. With mixed-valence bismuth oxides, $Bi_{0.7}Ba_{0.3}O_{1.5+\delta}$,[43] and $Bi_{0.6}Y_{0.4}O_{1.5+\delta}$,[44] increasing the effective oxygen partial pressure under preparation conditions (703 K, 5 h) causes a color changes from colorless to brown. The excess oxygen introduced under such oxidative conditions oxidize Bi(III) into Bi(V), enabling the charge-transfer band from Bi(III) $6s^2$ to Bi(V) $6s^0$, as in other post-transition metallic cation-containing mixed valence oxides [Pb(II)/Pb(IV) or Sb(III)/Sb(V)]. Other commercial catalysts for selective oxidation of propene [Fe−Sb−O or U−Sb−O],[45,46] contain antimony (Sb) in place of Bi, which probably plays a similar redox role.

We speculate that in an oxidizing environment an oxygen atom might react with a surface bismuth site, producing a very small amount of Bi(V). This new oxidized site would make H abstraction easier [with simultaneous reduction of Bi(V) to Bi-(III)]. We calculated the energy cost of (1) producing Bi(V) (Bi_4O_7) from Bi(III) (Bi_4O_6) (eq 6) and (2) abstracting hydrogen from propene by this new active site (eq 7)

$$Bi_4O_6 + \frac{1}{2}O_2(\text{or other oxygen source}) \rightarrow Bi_4O_7 \quad (6)$$

$$Bi_4O_7 + \text{propene} \rightarrow Bi_4O_7H + \text{allyl} \quad (7)$$

The optimized structures of the oxidized bismuth site and with hydrogen adsorbed on this site are shown in Figure 4, and the energy changes are listed in Table 4.

For this defect-like Bi(V) site, the free energy cost to extract the hydrogen from propene is just 2.5 kcal/mol. We propose that this oxidized bismuth site is the active site for the hydrogen abstraction from propene, as summarized in Scheme 1.

On the other hand, the free energy cost for formation of this Bi(V) active site by dissociative chemisorption of gas-phase oxygen molecule is fairly high, 36.9 kcal/mol. Although this is less than 41.6 kcal/mol for the H-abstraction by the conventional Bi(III) site, it still seems too high to be plausible. This energy cost includes half the dissociation free energy of oxygen into atomic oxygens. If the gas-phase oxygen molecule is dissociatively chemisorbed at some other site and the resulting atomic oxygen or oxide ion is transported to the Bi(III) site, the energy cost for the formation of active Bi(V) site might be lowered significantly. For example, Fe(II)/Fe(III) is known to serve as an efficient redox couple. The Fe(II) is capable of efficient dioxygen chemisorption and its reductive transformation to lattice oxygen, which can be transferred efficiently to the Bi−O−Mo active site. In fact, drastic improvement in catalyst performance has been achieved by adding Fe(II)/Fe(III). Thus, the tetracomponent Mo−Bi−Co−Fe−O catalyst shows the conversion of more than 90% of propene, whereas binary bismuth molybdate (α-$Bi_2Mo_3O_{12}$ and β-$Bi_2Mo_2O_9$) shows the conversion of only about 20% of propene.[3] Indeed it has been suggested that the excellent catalytic activity of this multicomponent catalyst is due to the enhanced activation of oxygen molecule by the Fe(II)/Fe(III) redox couple to atomic lattice oxygen, which migrates to the bismuth site.[3]

TABLE 4: Energy Change (kcal/mol) during the Oxidation of Bismuth Site and the H-abstraction from Propene to the Oxidized Bismuth Site

	ΔE	ΔZPE	$\Delta\Delta G_{0\rightarrow 673}$	ΔG_{673}
(a) $Bi_4O_6 + 0.5O_2 \rightarrow Bi_4O_7$	27.5	0.4	9.0	36.9
(b) $Bi_4O_7 + \text{propene} \rightarrow Bi_4O_7H + \text{allyl}$	6.4	−2.5	−1.4	2.5
(c) $Bi_4O_7H + \text{propene} \rightarrow Bi_4O_6 + H_2O + \text{allyl}$	−14.4	−2.2	−19.3	−35.9

However, we know of no spectroscopic evidence for the existence of Bi(V) on the bismuth molybdate catalysts. We speculate that this is because, once Bi(V) has been generated, it is consumed and restored to Bi(III) very quickly by reacting with another propene, a very exothermic process (−35.9 kcal/mol), as also summarized in Scheme 1

$$Bi_4O_7H + \text{propene} \rightarrow Bi_4O_6 + H_2O + \text{allyl} \quad (8)$$

3.1.4. MoO_2Cl_2 Model. In this section, we found that the Mo═O oxo oxygen in molybdate is much more active than the bridging oxygen (Mo−O−Mo). Thus, we expect that the oxo oxygen determine the critical steps of the reactions, making the bridging oxygens spectators that serve to stabilize the presence of the oxo oxygens. Thus, we suspected that the bridging oxygens could be replaced with chlorines as shown in Figure 2c in calculating the energetics without compromising the results. Replacing the model cluster Mo_3O_9 with MoO_2Cl_2 would make the calculations simpler and faster. To validate this simplification, we calculated the energy changes during several key reactions with these two model clusters (the larger one based on Mo_3O_9 and smaller one based on MoO_2Cl_2) (Appendix A). The simpler model MoO_2Cl_2 gives reasonable structures and energy changes when compared with the more complicated model Mo_3O_9. Thus, the following processes, allyl adsorption and oxygen insertion, were studied with this simpler model, MoO_2Cl_2. We should emphasize here that, experimentally, such a simplification could lead to quite different reactions. Using theory, we can examine just the chemistry at the oxo groups without considering side reactions that could be induced by the Cl.

3.2. Second Step: Allyl Adsorption. We expect that the allyl radical produced after the H abstraction by the active Bi(V)

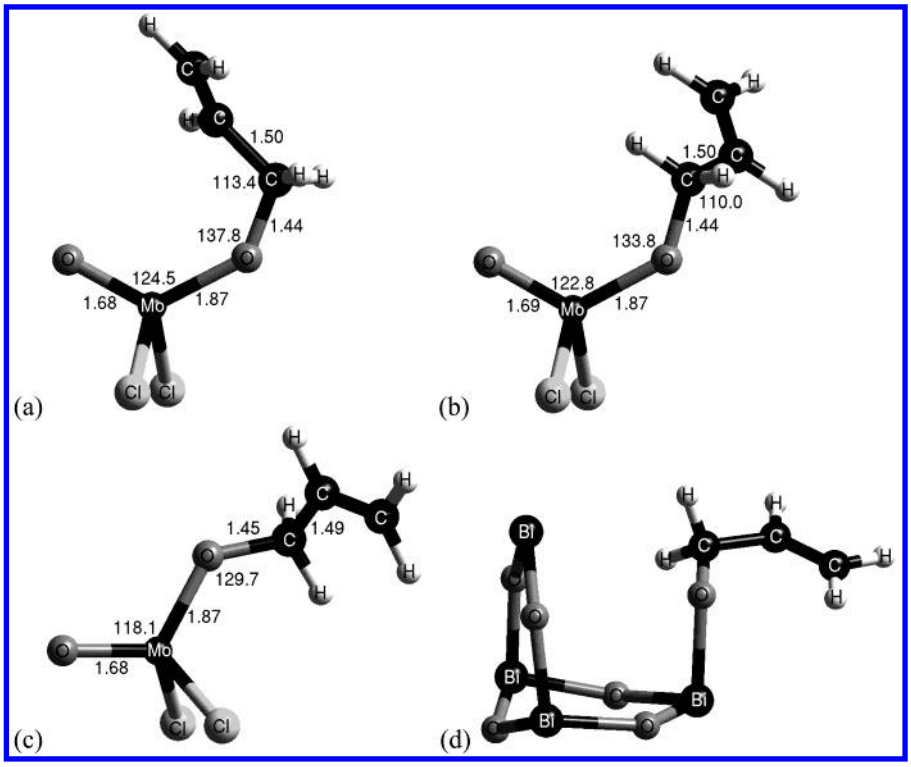

Figure 5. Optimized structures of allyl-adsorbed clusters. (a−c) The molybdenum site where the allyl radical is adsorbed in three different conformations (**5a**, **5b**, and **5c**) and (d) the allyl-adsorbed bismuth(III) site. Selected geometrical parameters (bond lengths and angles) are shown together in Å and in degrees, respectively.

TABLE 5: Energy Change (kcal/mol) during the Adsorption of the Allyl Radical (a−c) on Molybdenum Site in Three Different Conformation and (d) on Bismuth Site

	ΔE	ΔZPE	$\Delta\Delta G_{0\rightarrow 673}$	ΔG_{673}
(a) MoO_2Cl_2 + allyl → $MoOCl_2O\cdot\cdot CH_2CHCH_2$ (**5a**)	−20.5	3.6	23.6	6.7
(b) MoO_2Cl_2 + allyl → $MoOCl_2O\cdot\cdot CH_2CHCH_2$ (**5b**)	−20.3	3.6	23.2	6.5
(c) MoO_2Cl_2 + allyl → $MoOCl_2O\cdot\cdot CH_2CHCH_2$ (**5c**)	−21.5	3.6	23.7	**5.7**
(d) Bi_4O_6 + allyl → $Bi_4O_6\cdot\cdot CH_2CHCH_2$ ($41i$ cm^{-1})[a]	3.8	5.2	22.0	31.0

[a] The optimized structure is not a true minimum, as indicated by an imaginary frequency.

site is chemisorbed on a nearby active molybdenum or bismuth site. We exclude the possibility that the allyl radical finds another active bismuth site [Bi(V) or Bi(IV)]. This is because the concentration of Bi(V) is expected to be very low based on the endothermic oxidation reaction (37.0 kcal/mol), leading to a very low possibility of two adjacent Bi(V) sites. Also, a Bi-(IV) site is expected to react very quickly with other propenes which are present in much higher amount than allyl radicals, as discussed in section 3.1.3 (eq 8).

To determine which site is preferable for the allyl adsorption, we calculated the free energy cost of the following processes

$$\text{allyl} + MoO_2Cl_2 \rightarrow MoOCl_2O\cdot\cdot CH_2CHCH_2 \qquad (9)$$

$$\text{allyl} + Bi_4O_6 \rightarrow Bi_4O_6\cdot\cdot CH_2CHCH_2 \qquad (10)$$

There are several possible conformations of the adsorbed allyl group as shown in Figure 5. Only three representative conformations were considered: (a) the conformation where the α-carbon is cis with respect to the other oxo group and both α-hydrogens are away from the other oxo group of the molybdenum site (possibly located near to an oxo oxygen of an adjacent site), (b) the conformation where the α-carbon is cis with respect to the other oxo group and one of α-hydrogens is cis with respect to Mo, and (c) the conformation where the α-carbon is trans with respect to the other oxo group. The optimized structures of the allyl-adsorbed clusters are shown in Figure 5 and the energy costs of adsorption are given in Table 5.

TABLE 6: Bond Dissociation Enthalpies D_{298} (kcal/mol) at 298 K and Bond Dissociation Free Energies ΔG_{673} (kcal/mol) at 673 K of the C−H Bonds in the Allyl Group Adsorbed on the Molybdenum Site ($MoOCl_2O\cdot\cdot CH_2CHCH_2$; 5a), Leading to Two Different Spin States of $MoOCl_2OC_3H_4$

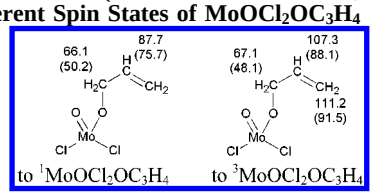

	leading to singlet		leading to triplet	
	D_{298}	ΔG_{673}	D_{298}	ΔG_{673}
$C_\alpha-H_\alpha$	66.1	50.2	**67.1**	**48.1**
$C_\beta-H_\beta$	87.7	75.7	107.3	88.1
$C_\gamma-H_\gamma$			111.2	91.5

Again, the allyl adsorption on the Bi(III) site results in the Bi−O bond cleavage, producing an unfavorable Bi(II), which leads to a high energy cost ($\Delta G_{673} \approx 31$ kcal/mol). However, the adsorption on the terminal oxo oxygen of the molybdenum site needs only moderate energy cost ($\Delta G_{673} = 5.7$ to 6.7 kcal/mol) for all three conformations. This indicates that the allyl radical is expected to adsorb preferably at the molybdenum site if a molybdenum site is available near the active bismuth site. This is the case on the bismuth molybdate catalysts (Figure 1c). In fact, it is consistent with the widely accepted "dual-site" concept that the allyl group produced on bismuth site adsorbs on molybdenum site.[5,6]

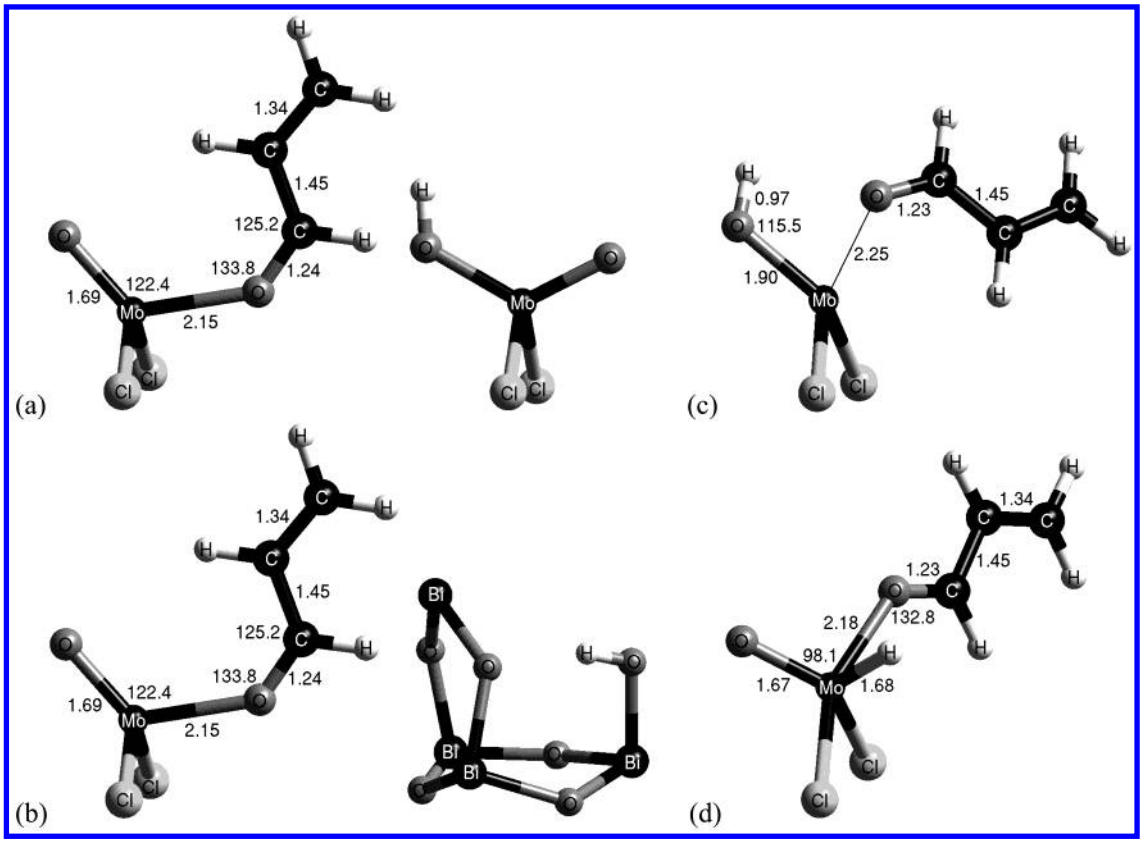

Figure 6. Optimized structures of the intermediates after the second H abstraction. (a−b) two-site transfer schemes starting from **5a**: (a) H transferred to an oxo group of an adjacent molybdenum site, (b) H transferred to an oxygen of an adjacent Bi(III) site. (c) Single-site transfer scheme starting from **5b**: H transferred to the other oxo group, and (d) single-site transfer scheme starting from **5c**: H transferred to the molybdenum center. Note that we show the most favorable structure of the products, while the reaction pathway might go through other intermediates on the way to this structure. Selected geometrical parameters (bond lengths and angles) are shown together in Å and in degrees, respectively.

SCHEME 2: Several Possible Pathways of the Second Hydrogen Abstraction. Energy Changes are Presented in kcal/mol. The Energetics are Shown in Detail in Table 7

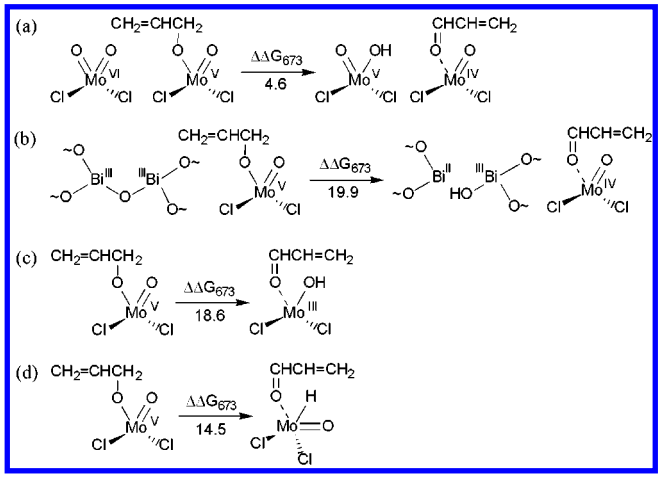

On the pure bismuth oxide (α-Bi_2O_3), however, the only site available for the allyl adsorption after the H abstraction is another bismuth site. The adsorption of the allyl radical on this site is not energetically stable, so that any further reaction other than dimerization of allyl radicals is disfavored. In fact, when propene is passed over α-Bi_2O_3, 1,5-hexadiene (the dimerization product) and benzene (its cyclization product) are the only major products.[5,47,48]

3.3. Third Step: Second H-Abstraction and Oxygen Insertion. The bond dissociation energy was calculated for various C−H bonds in the allyl group chemisorbed on MoO_2Cl_2 (Table 6). We find that the $C_\alpha-H_\alpha$ bond has weaken by 20 kcal/mol from the original $C_\alpha-H_\alpha$ bond of propene and now is more than 20 kcal/mol weaker than the other C−H bonds. Thus, after the allyl radical chemisorbs on an oxo group of a molybdenum site, we expect that a second α-hydrogen is abstracted by a second Mo═O of an adjacent site, producing a precursor of acrolein by simultaneous insertion of the first oxo oxygen into the allyl group.

TABLE 7: Energy Change (kcal/mol) during the Second Hydrogen Abstraction

	ΔE	ΔZPE	$\Delta\Delta G_{0\to673}$	ΔG_{673}
(a) $^2MoOCl_2O\cdot\cdot CH_2CHCH_2$ (**5a**) + MoO_2Cl_2 → $^3MoOCl_2\cdot\cdot OCHCHCH_2$ + $^2MoO(OH)Cl_2$	12.9	−1.5	−4.6	6.8
$^2MoOCl_2O\cdot\cdot CH_2CHCH_2$ (**5c**) + MoO_2Cl_2 → $^3MoOCl_2\cdot\cdot OCHCHCH_2$ + $^2MoO(OH)Cl_2$	10.6	−1.5	−4.5	4.6
(b) $^2MoOCl_2O\cdot\cdot CH_2CHCH_2$ (**5a**) + Bi_4O_6 → $^3MoOCl_2\cdot\cdot OCHCHCH_2$ + $^2Bi_4O_6H$	30.2	−0.9	−9.4	19.9
$^2MoOCl_2O\cdot\cdot CH_2CHCH_2$ (**5c**) + Bi_4O_6 → $^3MoOCl_2\cdot\cdot OCHCHCH_2$ + $^2Bi_4O_6H$	27.9	−0.9	−9.4	17.6
(c) $^2MoOCl_2O\cdot\cdot CH_2CHCH_2$ (**5b**) → $^4Mo(OH)Cl_2\cdot\cdot OCHCHCH_2$	21.4	−1.1	−1.7	18.6
(d) $^2MoOCl_2O\cdot\cdot CH_2CHCH_2$ (**5c**) → $^2MoHOCl_2\cdot\cdot OCHCHCH_2$	15.8	−2.3	1.0	14.5

There are several possible paths for the second α-hydrogen abstraction (Scheme 2 and Figure 6):

(a) H transfer to an oxo group of an adjacent molybdenum site

$$MoOCl_2O\cdot\cdot CH_2CHCH_2 + MoO_2Cl_2 \rightarrow MoOCl_2\cdot\cdot OCHCHCH_2 + MoO(OH)Cl_2, \quad (11)$$

TABLE 8: Energy Change (kcal/mol) during (a) Desorption of Acrolein and (b−c) Third H Abstraction

	ΔE	ΔZPE	$\Delta\Delta G_{0\rightarrow 673}$	ΔG_{673}
(a) $^3MoOCl_2\cdot\cdot OCHCHCH_2$ (from **5a**) → $^3MoOCl_2 + {}^1CH_2CHCHO$	17.2	−1.6	−25.2	−9.6
$^3MoOCl_2\cdot\cdot OCHCHCH_2$ (from **5c**) → $^3MoOCl_2 + {}^1CH_2CHCHO$	20.5	−1.5	−25.4	**−6.4**
(b) $^3MoOCl_2\cdot\cdot OCHCHCH_2$ (from **5a**) $+ {}^1MoO_2Cl_2$ → $^2MoOCl_2\cdot\cdot OCCHCH_2 + {}^2MoO(OH)Cl_2$	43.7	−2.0	−3.2	38.5
(c) $^3MoOCl_2\cdot\cdot OCHCHCH_2$ (from **5c**) $+ {}^1MoO_2Cl_2$ → $^2MoOCl_2\cdot\cdot OCCHCH_2 + {}^2MoO(OH)Cl_2$	49.3	−2.0	−4.1	43.1

SCHEME 3: Oxidation Part 1. Hydrogen Abstraction on Bismuth Site. Energy Changes are Presented in kcal/mol

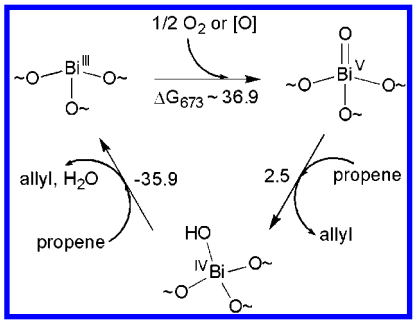

(b) H transfer to an oxygen of an adjacent bismuth site

$$MoOCl_2O\cdot\cdot CH_2CHCH_2 + Bi_4O_6 \rightarrow MoOCl_2\cdot\cdot OCHCHCH_2 + Bi_4O_6H \quad (12)$$

(c) H transfer to the other oxo group connected to the same molybdenum

$$MoOCl_2O\cdot\cdot CH_2CHCH_2 \rightarrow Mo(OH)Cl_2\cdot\cdot OCHCHCH_2 \quad (13)$$

or (d) H transfer to the molybdenum center

$$MoOCl_2O\cdot\cdot CH_2CHCH_2 \rightarrow MoHOCl_2\cdot\cdot OCHCHCH_2. \quad (14)$$

Paths (a) and (b) are accessible for conformations **5a** and **5c** where an α-hydrogen is placed only 1.5∼1.9 Å away from an oxo oxygen atom of an adjacent site (when the allyl group is positioned on α-MoO_3 surface when no reconstruction from its bulk structure is assumed), path (c) for **5b**, and path (d) for **5c**. Again, we exclude the possibility that the hydrogen is abstracted by another active bismuth site [Bi(V) or Bi(IV)] as discussed in section 3.2.

Figure 7. Model cluster $MoOCl_2$ representing the reduced molybdenum site Mo(IV). Mo═O bond length is shown together in Å.

The calculated free energy cost necessary for each path is given in Table 7. We find that the most favorable mechanism for extracting the second hydrogen is path (a), to an oxo group of an adjacent molybdenum site (two-site scheme; $\Delta G_{673} = 4.6$ kcal/mol from **5c** or 6.8 kcal/mol from **5a**). Thus, we expect that at least two adjacent molybdenum sites are necessary for the most favorable reaction, as suggested by Allison and Goddard.[7] Indeed some of the bismuth molybdate catalysts have this structure in the bulk phase (e.g., α-$Bi_2Mo_3O_{12}$[10,11] shown schematically in Figure 1c), whereas in others it may be introduced in the surface.

3.4. Fourth Step: Acrolein Desorption. After the second hydrogen abstraction, there are two likely possibilities in further reactions of $^3MoOCl_2\cdot\cdot OCHCHCH_2$:

(a) desorption of the acrolein or

(b) the third H abstraction.

The desorption of acrolein is exothermic (Table 8a). Acrolein can desorb easily at this stage, leaving behind $^3MoOCl_2$ (Figure 7). On the other hand, the energy cost of further C_α-H_α activation is so high (Table 8b) that the third α-hydrogen abstraction is not likely to happen.

3.5. Reoxidation. The reduced Mo(IV) site [$^3MoOCl_2$] left behind the acrolein desorption must be reoxidized in order to regain the intial state

$$MoOCl_2 + \frac{1}{2}O_2(\text{or other oxygen source}) \rightarrow MoO_2Cl_2 \quad (15)$$

The Mo(V) sites [$MoO(OH)Cl_2$] produced by abstracting

SCHEME 4: Oxidation Part 2. Allyl Adsorption, Oxygen Insertion, and Reoxidation on Molybdenum Site. Energy Changes are Presented in kcal/mol

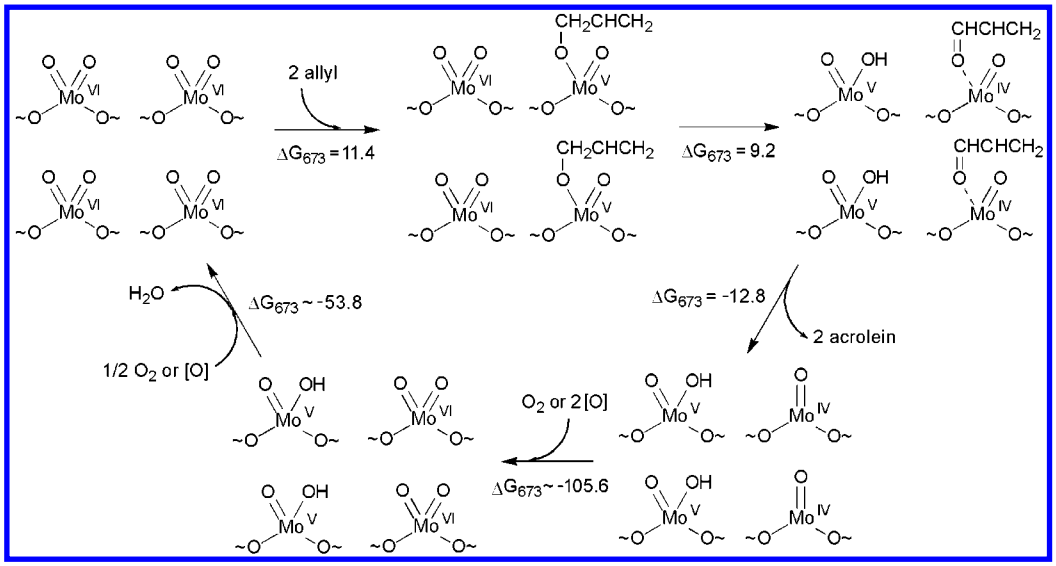

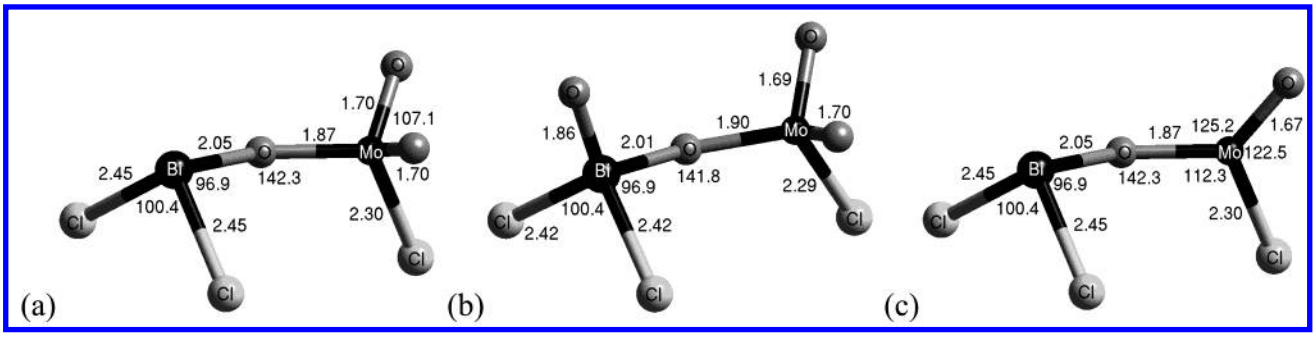

Figure 8. Optimized structures of two-site, mixed clusters. (a) $^1\{Bi^{III}Cl_2-O-Mo^{VI}O_2Cl\}$, (b) $^1\{O{=}Bi^{V}Cl_2-O-Mo^{VI}O_2Cl\}$, an oxidized site, and (c) $^3\{Bi^{III}Cl_2-O-Mo^{IV}O_2Cl\}$, a reduced site. Selected geometrical parameters (bond lengths and angles) are shown together in Å and in degrees.

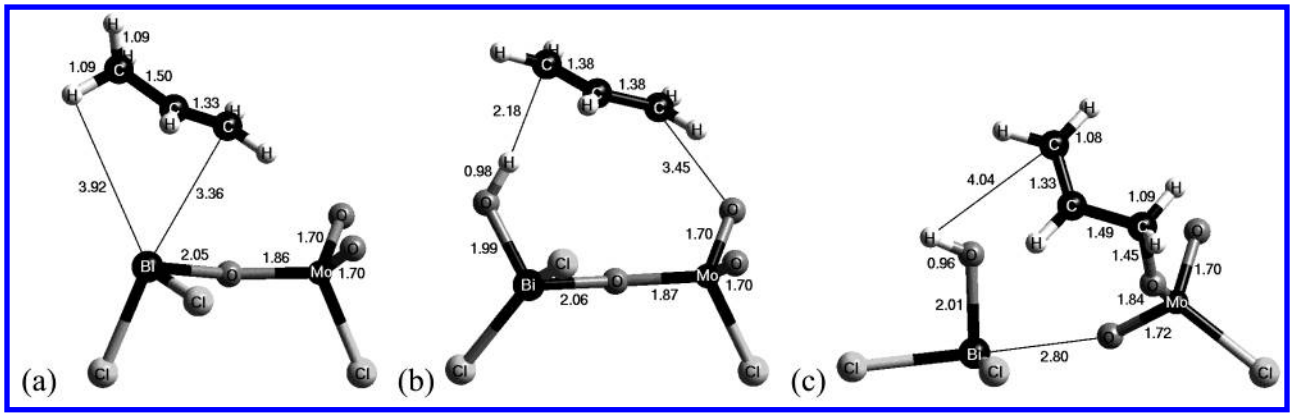

Figure 9. Structures obtained from a geometry optimization started from a propene placed close to two-site model clusters. (a) Propene on the normal oxidation-state cluster, $^1\{Propene{\cdot\cdot}Bi^{III}Cl_2-O-Mo^{VI}O_2Cl\}$, (b−c) Propene on the oxidized cluster, $^3\{propene{\cdot\cdot}O{=}Bi^{V}Cl_2-O-Mo^{VI}O_2Cl\}$ (b) and $^1\{propene{\cdot\cdot}O{=}Bi^{V}Cl_2-O-Mo^{VI}O_2Cl\}$ (c). Selected geometrical parameters (bond lengths and angles) are shown together in Å and in degrees.

SCHEME 5: Several Possible Configurations of Dissociative Adsorption of Propene on a Two-site, Mixed Cluster Model, $Bi^{III}Cl_2-O-Mo^{VI}O_2Cl$

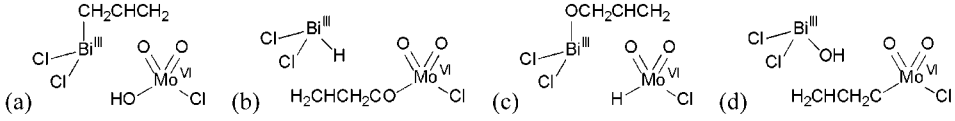

TABLE 9: Energy Change (kcal/mol) during the Reoxidation

	ΔE	ΔZPE	$\Delta\Delta G_{0\rightarrow 673}$	ΔG_{673}
(a) $^3MoOCl_2 + 0.5O_2 \rightarrow$ $^1MoO_2Cl_2$	−68.5	1.3	14.4	−52.8
(b) $2\ ^2MoO(OH)Cl_2 + 0.5O_2 \rightarrow$ $2\ ^1MoO_2Cl_2 + H_2O$	−47.6	0.1	−6.2	−53.7

hydrogens from allyl groups adsorbed on adjacent molybdenum sites (section 3.3) can be reoxidized through dehydration

$$2\ MoOCl_2(OH) + \frac{1}{2}O_2(\text{or other oxygen source}) \rightarrow 2\ MoO_2Cl_2 + H_2O \quad (16)$$

The energy changes during these processes are given in Table 9. Again, there might be other sources of atomic oxygen species (e.g., lattice oxygen) that would change the energy cost shown in Table 9. In any case, this reoxidation of molybdenum is very exothermic. We speculate that this exothermic reoxidation of molybdenum site could be coupled with the oxidation of bismuth site from Bi(III) to Bi(V). This exothermic reoxidation of molybdenum site could be a driving force to draw lattice oxygens generated remotely, placing them nearby a bismuth would favor oxidizing the Bi.

SCHEME 6: Most Plausible Configuration of Dissociative Adsorption of Propene on an Oxidized Two-site Cluster $O{=}Bi^{V}Cl_2-O-Mo^{VI}O_2Cl$, in Each Spin State, Triplet (b) and Singlet (c), and the Initial Adsorption Configuration Leading to Them (a)[a]

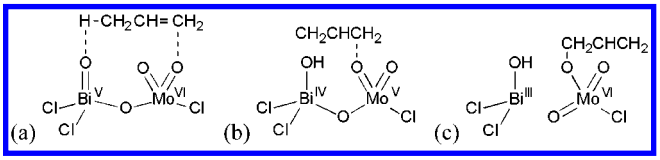

[a] The distance between two adsorption sites (Bi=O and Mo=O) in (a) is 4.68 Å.

3.6. Summary: Oxidation. We conclude that activation of the propene requires a Bi(V) site, whereas all subsequent reactions involve di-oxo Mo(VI) sites adjacent to the Bi. We find that two such Mo sites are required for the most favorable reactions. These results are compatible with current experimental data. The reaction mechanism with the most favorable energetics (through conformation **5c**) is summarized in Schemes 3 and 4. The final reaction equation is

$$CH_3CHCH_2 + O_2 \rightarrow CH_2CHCHO + H_2O$$

$$\Delta G_{673} = -74.0\ \text{kcal/mol}\ (-72.8\ \text{kcal/mol at 298 K})$$

SCHEME 7: Desorption of Acrolein and Water, Leaving Behind the Reduced Two-Site Model Cluster, $Bi^{III}Cl_2-O-Mo^{IV}OCl$

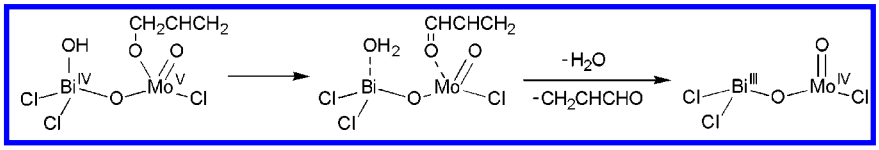

SCHEME 8: Reoxidation of the Reduced Cluster, $Bi^{III}Cl_2-O-Mo^{IV}OCl$[a]

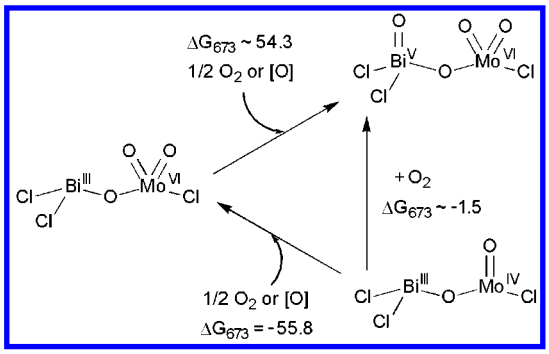

[a] It should be noted that the energy costs of oxidation at the bismuth site calculated on this cluster (54.3 kcal/mol) and on $BiCl_3$ (48.8 kcal/mol) are much higher than the corresponding value calculated on Bi_4O_6 cluster (36.9 kcal/mol). It implies that this cluster represents the reaction site only qualitatively and that the energy costs listed in this scheme is the upper limit of the real value.

4. Two-Site, Mixed Cluster Models

In earlier sections, the reaction sites were represented by separate, single-site clusters of bismuth molybdates (Bi_4O_6, Mo_3O_9, and MoO_2Cl_2) for conceptual simplicity. We also assumed a sequential reaction scheme rather than a concerted one. That is, it was assumed that the first hydrogen abstraction produces a hydrogen atom adsorbed on a surface site and a gas-phase allyl radical ($CH_2{=}CHCH_2{\cdot}$), followed by the adsorption of the allyl radical on another surface site.

It is also plausible that a propene is dissociated into a hydrogen atom and an allyl group both adsorbed on surface sites. In this section, this alternative reaction scheme—C-H activation by dissociative adsorption of propene on bismuth molybdates—was investigated on a two-site cluster model for bismuth molybdates. On the basis of the calculation results shown in earlier sections and the widely accepted "dual-site" concept,[5,6] it is expected that the hydrogen atom adsorbs on the bismuth site and the allyl on the molybdenum site. Thus, a mixed cluster composed of a bismuth site and a molybdenum site ($^1\{Bi^{III}Cl_2-O-Mo^{VI}O_2Cl\}$, Figure 8a) was chosen as the two-site model cluster. In this cluster, each oxide is terminated by chlorine atoms ($-BiCl_2$ and $-MoO_2Cl$) except the oxygen atom bridging Bi and Mo. The oxidized and reduced clusters ($^1\{O{=}Bi^{V}Cl_2-O-Mo^{VI}O_2Cl\}$ and $^3\{Bi^{III}Cl_2-O-Mo^{IV}O_2Cl\}$) are also shown in Figure 8b and 8c, respectively.

4.1. Dissociative Adsorption of Propene on $Bi^{III}Cl_2-O-Mo^{VI}O_2Cl$. Several plausible configurations after the dissociative adsorption of propene on $Bi^{III}Cl_2-O-Mo^{VI}O_2Cl$ are schematically shown in Scheme 5. Because any of these configurations do not produce an unfavorable oxidation state [Bi(II) or Mo(V)], we expected that all of them could be at least moderately favorable. However, all the processes were found to be very endothermic ($\Delta G_{673} > 40$ kcal/mol), probably because (1) the entropy decreases a great deal due to adsorption of the gas-phase propene and (2) the new Bi−H, Bi−C, Mo−H, and Mo−C bonds are not strong enough to compensate the cleavage of C−H, Bi−O, and Mo−O bonds.

In fact, a geometry optimization started from a propene placed close to the cluster only led to two separate species (Figure 9a). A stable adsorption structure was not found.

Here, we confirm again one of our conclusions drawn from separated, single-site model clusters: a bismuth site and molybdenum site at their normal oxidation states [Bi(III) and Mo(VI)] are not likely to activate the C−H bond of propene.

4.2. Dissociative Adsorption of Propene on an Oxidized Cluster ($O{=}Bi^{V}Cl_2-O-Mo^{VI}O_2Cl$). However, when a propene was placed close to the oxidized cluster, $O{=}Bi^{V}Cl_2-O-Mo^{VI}O_2Cl$ (Figure 8b), as in Scheme 6a, geometry optimization directly led to a final configuration where an α-hydrogen of propene was abstracted by the bismuth oxo oxygen. Figure 9b and 9c show the final structures in different spin states, triplet and singlet, respectively. Their schematic structures are given in Scheme 6b and 6c.

This would be followed by the second hydrogen abstraction from the adsorbed allyl group. In this two-site model, we can see another possible path other than an abstraction by an Mo=O nearby: a hydrogen abstraction by Bi−OH (Scheme 7). This might also be implausible because Bi−OH is so reactive that it would not wait until the $C_\alpha-H_\alpha$ bond is positioned at the proper configuration to be broken by the Bi−OH group. Any case of second hydrogen abstraction would be followed by desorption of water and acrolein (Scheme 7), and the reduced cluster $Bi^{III}Cl_2-O-Mo^{IV}OCl$ would be left behind and should be reoxidized.

4.3. Reoxidation of a Reduced Cluster ($Bi^{III}Cl_2-O-Mo^{IV}OCl$). Whereas the oxidation of Bi(III) to Bi(V) is very

SCHEME 9: Oxidation in a Two-site Cluster Model

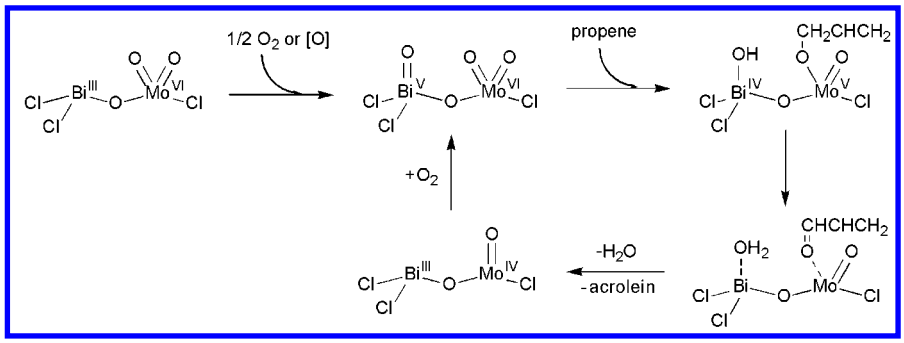

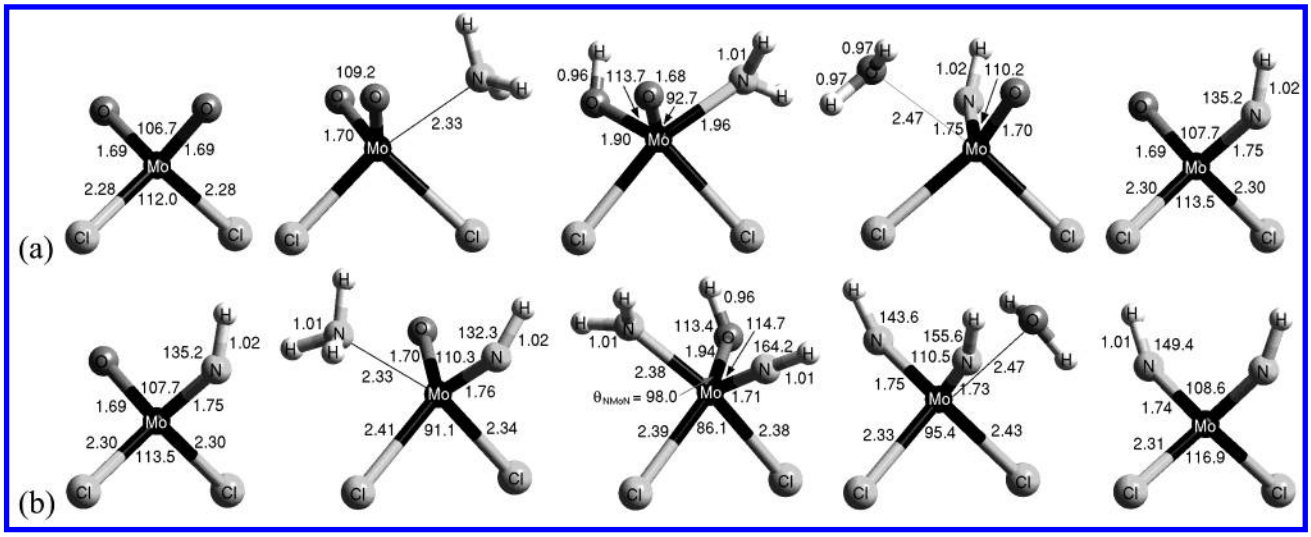

Figure 10. Optimized structures for intermediates during ammonia activation. (a) Ammonia adsorption on MoO_2Cl_2, intramolecular hydrogen transfer leading to desorption of water, and the resulted $MoO(NH)Cl_2$. (b) Ammonia adsorption $MoO(NH)Cl_2$, intramolecular hydrogen transfer leading to the desorption of water, and the resulted $Mo(NH)_2Cl_2$. Selected geometrical parameters (bond lengths and angles) are shown together in Å and in degrees, respectively.

SCHEME 10: Activation of the First Ammonia to Generate $MoO(NH)Cl_2$ from Mo(VI) Represented as MoO_2Cl_2

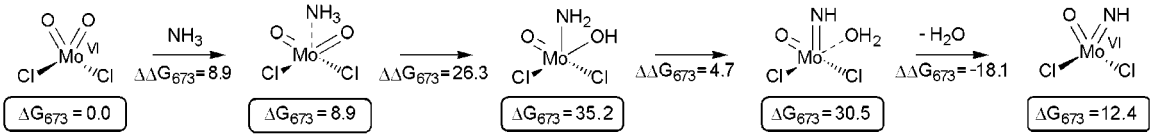

TABLE 10: Energy Change (kcal/mol) during Ammonia Activation on Mo(VI) Represented as MoO_2Cl_2

(a) 1st ammonia activation to generate $MoO(NH)Cl_2$	ΔE	ΔZPE	$\Delta\Delta G_{0\rightarrow 673}$	ΔG_{673}
$MoO_2Cl_2 + NH_3 \rightarrow MoO_2Cl_2\cdot\cdot NH_3$	−16.7	3.1	22.5	8.9
$MoO_2Cl_2\cdot\cdot NH_3 \rightarrow MoO(OH)Cl_2(NH_2)$	28.8	−2.0	−0.5	26.3
$MoO(OH)Cl_2(NH_2) \rightarrow MoO(NH)Cl_2\cdot\cdot OH_2$	−4.5	−0.1	−0.1	−4.7
$MoO(NH)Cl_2\cdot\cdot OH_2 \rightarrow MoO(NH)Cl_2 + H_2O$	6.1	−2.4	−21.8	−18.1
(net) $MoO_2Cl_2 + NH_3 \rightarrow MoO(NH)Cl_2 + H_2O$	13.7	−1.4	0.1	12.4

(b) 2nd ammonia activation to generate $Mo(NH)_2Cl_2$	ΔE	ΔZPE	$\Delta\Delta G_{0\rightarrow 673}$	ΔG_{673}
$MoO(NH)Cl_2 + NH_3 \rightarrow MoO(NH)Cl_2\cdot\cdot NH_3$	−13.5	3.0	23.7	13.1
$Mo(NH)Cl_2\cdot\cdot NH_3 \rightarrow Mo(OH)(NH)Cl_2(NH_2)$	28.7	−2.0	−0.7	26.0
$Mo(OH)(NH)Cl_2(NH_2) \rightarrow Mo(NH)_2Cl_2\cdot\cdot OH_2$	−1.6	−0.4	−1.1	−3.1
$Mo(NH)_2Cl_2\cdot\cdot OH_2 \rightarrow Mo(NH)_2Cl_2 + H_2O$	2.8	−2.2	−21.1	−20.6
(net) $MoO(NH)Cl_2 + NH_3 \rightarrow Mo(NH)_2Cl_2 + H_2O$	16.4	−1.6	0.8	15.4

endothermic (ΔG_{673} < 54.3 kcal/mol; Scheme 8), it is almost thermoneutral ($\Delta G_{673} \approx -1.5$ kcal/mol; Scheme 8) when it is coupled with another very exothermic reaction, the reoxidation of Mo(IV) to Mo(VI) ($\Delta G_{673} \approx -55.8$ kcal/mol), as pointed out earlier in section 3.5. We conclude that the oxidation of Bi, the C−H bond dissociation and subsequent events occur together concertedly.

4.4. Summary: Oxidation of a Two-Site Cluster Model. On the two-site cluster model, we can develop much simpler reaction cycle (Scheme 9). This scheme does not necessarily need two adjacent Mo sites to abstract the second hydrogen from the adsorbed allyl group. However, we cannot estimate reliable energy changes for this cycle since the Cl-termination of the bismuth site is not a good representation.

5. Ammoxidation

For ammoxidation we investigated (1) ammonia activation on a molybdenum site to generate imido groups, (2) allyl adsorption on these imido sites, and (3) N-insertion into the adsorbed allyl group. The single-site cluster model of the molybdenum site was used. Because the hydrogen abstraction from propene is believed to occur on bismuth site, we assumed that this process is not affected by the presence of ammonia and did not investigate this step again.

5.1. Ammonia Activation. First we calculated the energetics of each step involved in ammonia activation on a single molybdenum site. The most abundant molybdenum species is Mo(VI), and this was represented by a model cluster MoO_2Cl_2 (Figure 2c). The activation of the first ammonia (Figure 10a) would proceed via

(a) ammonia adsorption on MoO_2Cl_2,

(b) transfer of hydrogens from ammonia to an oxo group, and

(c) desorption of water leaving behind the imido group, $MoO(NH)Cl_2$.

The activation of the second ammonia (Figure 10b) would proceed in the same way, except that it starts from $MoO(NH)Cl_2$ and ends up with $Mo(NH)_2Cl_2$. The optimized structures of intermediates are shown in Figure 10 and the energy changes are given in Table 10. The activation process of the first ammonia is summarized in Scheme 10.

The overall energy cost (ΔG_{673}) is 12.4 kcal/mol for the first ammonia activation and 15.4 kcal/mol for the second ammonia activation. The processes are quite endothermic and the second activation is harder than the first one. The ammonia adsorption is not easy ($\Delta G_{673} = 8.9$ for the first ammonia and 13.1 kcal/

SCHEME 11: Activation of the First Ammonia on Mo(IV) Represented as $MoOCl_2$

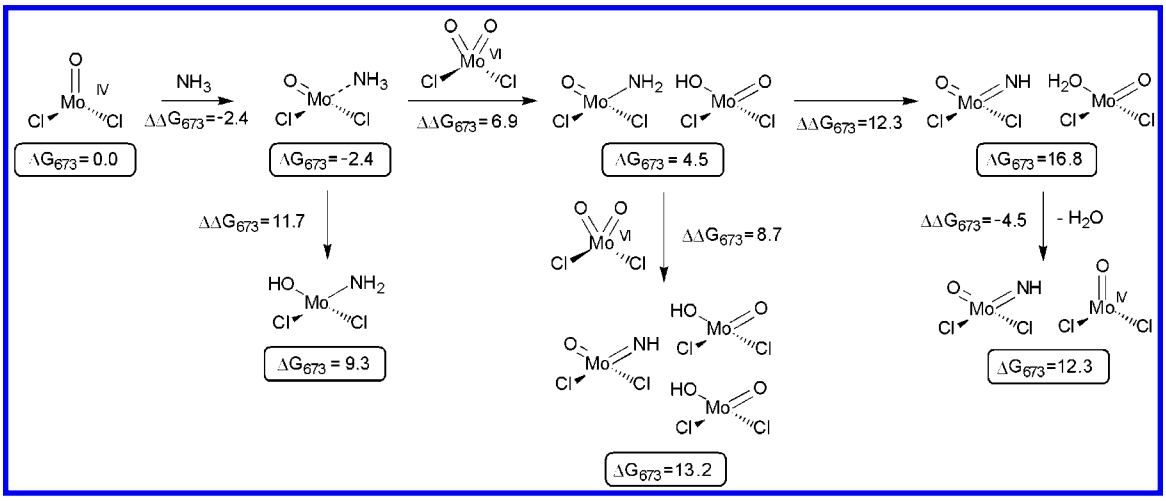

TABLE 11: Energy Change (kcal/mol) during Ammonia Activation on Mo(IV) Represented as $MoOCl_2$

(a) 1st ammonia activation to generate $MoO(NH)Cl_2$	ΔE	ΔZPE	$\Delta\Delta G_{0\rightarrow673}$	ΔG_{673}
$MoOCl_2 + NH_3 \rightarrow$ $MoOCl_2\cdot\cdot NH_3$	−28.5	2.9	23.2	**−2.4**
$MoOCl_2\cdot\cdot NH_3 + MoO_2Cl_2 \rightarrow$ $MoOCl_2(NH_2) + MoO(OH)Cl_2$	10.1	−2.1	−1.1	**6.9**
$MoOCl_2(NH_2) + MoO(OH)Cl_2 \rightarrow$ $MoO(NH)Cl_2 + MoOCl_2\cdot\cdot OH_2$*	12.2	0.2	−0.2	**12.3**
$MoOCl_2\cdot\cdot OH_2 \rightarrow$ $MoOCl_2 + H_2O$	19.8	−2.5	−21.8	**-4.5**
(net) $MoO_2Cl_2 + NH_3 \rightarrow$ $MoO(NH)Cl_2 + H_2O$	13.6	−1.5	0.1	**12.3**

mol for the second ammonia), and the first hydrogen transfer from the adsorbed ammonia to an adjacent oxo group costs as much as 26 kcal/mol for both cases. These processes seem too endothermic to be plausible.

Since ammonia is a well-known reducing agent, there might be a significant amount of reduced molybdenum sites in the presence of ammonia. The presence of propene could also generate reduced molybdenum sites, Mo(IV), in the course of its oxidation to acrolein, prior to ammoxidation. We speculated that the ammonia activation could be easier on this reduced Mo(IV) site which can be represented by $MoOCl_2$ (Figure 7). This is because this site has one open adsorption site, making the ammonia adsorption easier than on MoO_2Cl_2. Moreover, whereas one of the oxo groups should be removed from $MoO_2Cl_2\cdot\cdot NH_3$ and the hydrogen transfer from ammonia should be intramolecular in the ammonia activation involving Mo(VI) site (Figure 10), the oxo group would not have to be removed from $MoOCl_2\cdot\cdot NH_3$ in the ammonia activation involving Mo(IV) site and the hydrogen could be transferred from ammonia to an oxo group of an adjacent molybdenum site (Scheme 11), making this process easier. Thus, we calculated the energetics of

SCHEME 12: Model of Activation of Ammonia and Propene over Molybdate, Proposed by Grasselli and Coworkers. Adapted from Ref 49

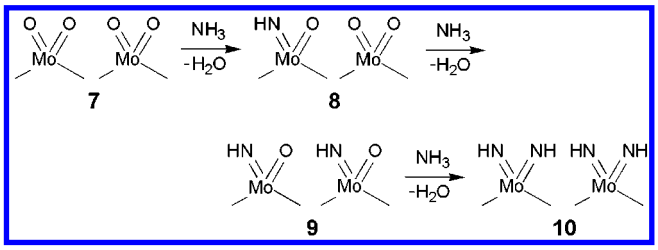

ammonia activation on a reduced molybdenum site Mo(IV): (1) the ammonia adsorption on $MoOCl_2$ and (2) hydrogen transfer from ammonia to an oxo group of an adjacent molybdenum site (Table 11). Optimized structures of intermediates are shown in Figure 11.

The net energy cost is the same (12.3 kcal/mol), but the energy cost of each step was reduced greatly for Mo(IV). As expected, the ammonia adsorption is now exothermic (−2.4 kcal/mol) on Mo(IV) and the first hydrogen transfer costs only 6.9 kcal/mol by the aid of an adjacent molybdenum site. The second hydrogen transfer is now the least favorable (rate-determining) step, and the energy cost (12.3 kcal/mol) is much smaller than the 26 kcal/mol of the rate-determining step on Mo(VI). This energy cost could be reduced even more to 8.7 kcal/mol, if one more adjacent molybdenum site is present nearby with its oxo group playing a role as a second hydrogen acceptor. These results indicate that ammonia activation is much easier under reducing conditions, for example, at higher partial pressures of ammonia and propene.

These results are consisitent with experimental findings of Grasselli and co-workers on the kinetic behavior of ammonia activation and their interpretation.[49] From a kinetic study on

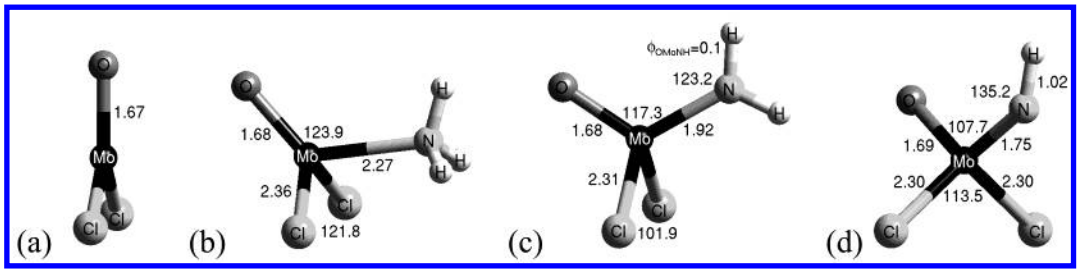

Figure 11. Optimized structures for intermediates during ammonia activation on $MoOCl_2$. Selected geometrical parameters (bond lengths and angles) are shown together in Å and in degrees, respectively.

SCHEME 13: Allyl Adsorption on Various Molybdenum Sites

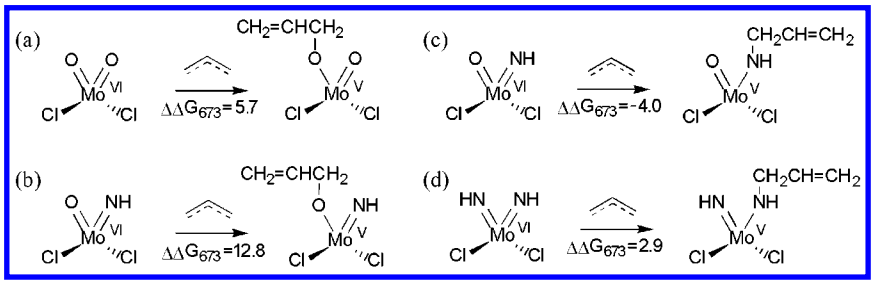

the ammoxidation process, they found that the relationship between the ammonia/propene feed ratio and the acrylonitrile/acrolein product ratio depends on the partial pressure of reactants in the feed. At low partial pressures of feed ($pC_3H_6 = 0.041$ atm), the product ratio is a linear function of NH_3/C_3H_6, indicating that one ammonia molecule is involved at the N-insertion site per catalytic cycle. At intermediate and high partial pressures of feed ($pC_3H_6 = 0.082$ and 0.14 atm), the product ratio is a linear function of $(NH_3)^2/C_3H_6$, corresponding to two ammonia molecules activated at the N-insertion site per acrylonitrile formed.

They interpreted this by assuming different active sites at different partial pressures of feed (Scheme 12).[49] At low partial pressures of feed ($pC_3H_6 = 0.041$ atm), the major surface species involved in N-insertion is a low concentration of "oxo-imido" species surrounded by abundant "oxo-oxo"species (**8** in Scheme 12). At intermediate partial pressures of feed ($pC_3H_6 = 0.082$ atm), it is a high concentration of "oxo-imido" species, which are now present next to each other (**9** in Scheme 12). At higher partial pressures of feed ($pC_3H_6 = 0.14$ atm), "imido-imido" species (**10** in Scheme 12) are the major N-inserting species. That is, "imido" groups generated by the ammonia activation are more abundant in higher partial pressure of feeds (ammonia and propene), that is, in more reducing conditions. Our calculations lead to independent confirmation of this interpretation.

5.2. Allyl Adsorption. In Table 12 and Scheme 13, we compare the calculated energetics for adsorption of an allyl radical on (a) the oxo group of "oxo-oxo" discussed in the section on oxidation with (b) the imido group of the "oxo-imido" species, (c) the oxo group of the "oxo-imido" species, and (d) an imido group of the "imido-imido" species.

Comparing (a) with (c), we can see that the allyl adsorption is 10 kcal/mol more favorable on an imido group than on an oxo group (Both contains an oxo spectator group). Similarly comparing (b) with (d) we also find that allyl adsorption is 10 kcal/mol more favorable on an imido group than on an oxo group (Both contains an imido spectator group).

Comparing (a) and (b), where the allyl adsorbs on the same oxo group, we see that a spectator oxo group is stabilizing the adsorbed allyl 7 kcal/mol more than that of a spectator imido group. Similarly comparing (c) and (d), where the allyl adsorbs on the same imido group, we also find that the spectator effect

TABLE 12: Energy Change (kcal/mol) during the Adsorption of an Allyl Radical on Various Molybdenum Sites[a]

	ΔE	ΔZPE	$\Delta\Delta G_{0\rightarrow673}$	ΔG_{673}
(a) MoO_2Cl_2 + allyl → $MoOCl_2O$··allyl	−21.5	3.6	23.7	5.7
(b) $MoO(NH)Cl_2$ + allyl → $Mo(NH)Cl_2O$··allyl (allyl on oxo)	−14.4	3.3	23.8	12.8
(c) $MoO(NH)Cl_2$ + allyl → $MoOCl_2(NH)$··allyl (allyl on imido)	−34.3	4.8	25.5	−4.0
(d) $Mo(NH)_2Cl_2$ + allyl → $Mo(NH)Cl_2(NH)$··allyl	−26.5	4.3	25.1	2.9

[a] Note that the same results were reported earlier.[50] However, all numbers shown in row (b) were interchanged with all numbers shown in row (c).

TABLE 13: Bond Dissociation Enthalpies D_{298} (kcal/mol) at 298 K and Bond Dissociation Free Energies (kcal/mol) at 673 K of the $C_\alpha-H_\alpha$ and N−H Bonds in $MoOCl_2NH$··CH_2CHCH_2 (12a)

	leading to singlet		leading to triplet	
	D_{298}	ΔG_{673}	D_{298}	ΔG_{673}[a]
$C_\alpha-H_\alpha$	58.49	42.2	59.0	40.7
N−H	58.04	42.2	102.2	81.3

[a] Corresponding values for $MoNHCl_2NH$··CH_2CHCH_2 are 39.8 for $C_\alpha-H_\alpha$ and 100.6 for N−H.

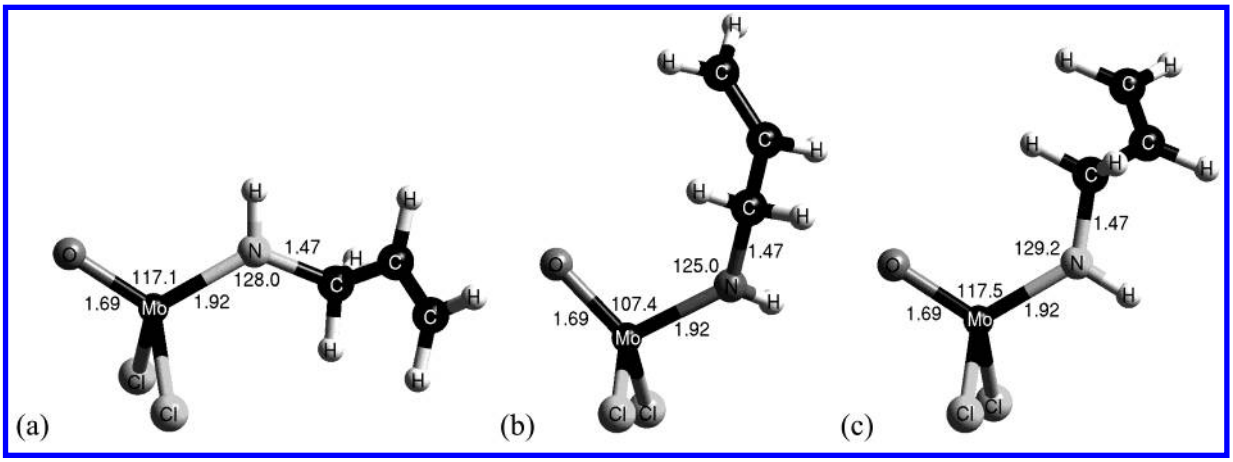

Figure 12. Optimized structures of $MoO(NH)Cl_2$ where an allyl radical is adsorbed on the imido group in three different conformations (**12a**, **12b**, and **12c**). Selected geometrical parameters (bond lengths and angles) are shown together in Å and in degrees, respectively. The adsorption free energies ΔG_{673} are −4.0, −2.4, and −3.3 kcal/mol for **12a**, **12b**, and **12c**, respectively.

TABLE 14: Energy Change (kcal/mol) during the Second Hydrogen Abstraction from the $C_\alpha-H_\alpha$ Bond of the $MoOCl_2NH\cdot\cdot CH_2CHCH_2$ (12a)

	ΔE	ΔZPE	$\Delta\Delta G_{0\rightarrow673}$	ΔG_{673}
(a) $^2MoOCl_2NH\cdot\cdot CH_2CHCH_2$ + $MoO(NH)Cl_2 \rightarrow$ $^3MoOCl_2\cdot\cdot NHCHCHCH_2$ + $^2MoO(NH_2)Cl_2$	−6.9	0.0	−2.4	**−9.2**
(b) $^2MoOCl_2NH\cdot\cdot CH_2CHCH_2$ + $MoO_2Cl_2 \rightarrow$ $^3MoOCl_2\cdot\cdot NHCHCHCH_2$ + $^2MoO(OH)Cl_2$	4.3	−1.0	−3.8	−0.5
(c) $^2MoOCl_2NH\cdot\cdot CH_2CHCH_2 \rightarrow$ $^4Mo(OH)Cl_2\cdot\cdot NHCHCHCH_2$	19.3	−0.8	−2.2	16.4
(d) $^2MoOCl_2NH\cdot\cdot CH_2CHCH_2 \rightarrow$ $^2MoHOCl_2\cdot\cdot NHCHCHCH_2$	9.6	−2.1	−2.2	7.2

SCHEME 14: Several Possible Pathways of the Second H Abstraction in the Course of Ammoxidation on the "Oxo-Imido" Site

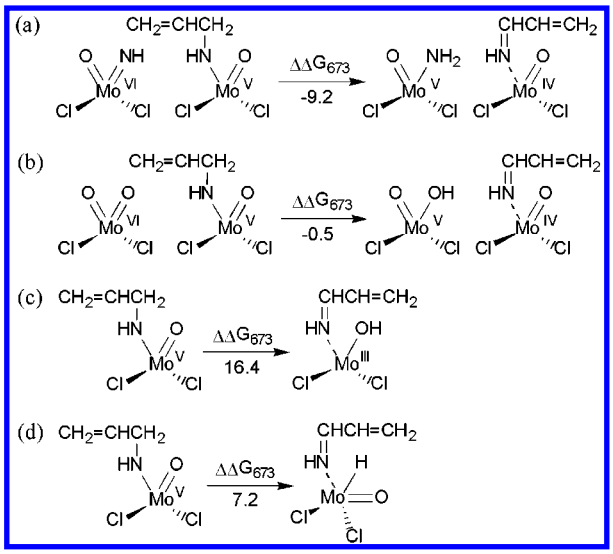

of an oxo group is 7 kcal/mol larger than that of a spectator imido group. This is consistent with the earlier work of Allison and Goddard[7] who showed the difference in spectator oxo and imido effect to be 15 kcal/mol.

These results are consistent with the assumption that Grasselli and co-workers made to derive kinetic equations for ammoxidation.[49] They assumed that N insertion is favored over O insertion. Considering that the allyl adsorption is the major part of the O- or N-insertion process, the lower energy cost for the allyl adsorption on an imido group [case (b); −4.0 kcal/mol] than on an oxo group [case (c); 12.8 kcal/mol] confirms this assumption. They also assumed that O insertion from di-oxo is easier than from oxo-imido. Lower energy cost for the allyl adsorption on an oxo group of the "oxo-oxo" species [case (a); 5.7 kcal/mol] than on an oxo group of the "oxo-imido" species [case (c); 12.8 kcal/mol] confirms this assumption.

TABLE 15: Energy Change (kcal/mol) during the Second Hydrogen Abstraction from the $C_\alpha-H_\alpha$ Bond of the $Mo(NH)Cl_2NH\cdot\cdot CH_2CHCH_2$

	ΔE	ΔZPE	$\Delta\Delta G_{0\rightarrow673}$	ΔG_{673}
(a) $^2Mo(NH)Cl_2NH\cdot\cdot CH_2CHCH_2$ + $MoO(NH)Cl_2 \rightarrow$ $^3Mo(NH)Cl_2\cdot\cdot NHCHCHCH_2$ + $^2MoO(NH_2)Cl_2$	−2.2	−0.3	−4.0	−6.5
(b) $^2Mo(NH)Cl_2NH\cdot\cdot CH_2CHCH_2 \rightarrow$ $^4Mo(NH_2)Cl_2\cdot\cdot NHCHCHCH_2$	−7.0	1.3	0.9	−4.8
(c) $^2Mo(NH)Cl_2NH\cdot\cdot CH_2CHCH_2 \rightarrow$ $^2MoH(NH)Cl_2\cdot\cdot NHCHCHCH_2$	5.3	−1.5	0.5	4.3

Another implication from these calculations is that the most favorable site for ammoxidation (at least for the allyl adsorption) would be the "oxo-imido" one. The allyl adsorption on the imido group of this site was the most favorable among various adsorption possibilities. Several possible conformations of the adsorbed allyl group on this site [$MoOCl_2(NH)\cdot\cdot$allyl] are shown in Figure 12. Because the adsorption geometries of $Mo(NH)Cl_2O\cdot\cdot$allyl and of $Mo(NH)Cl_2(NH)\cdot\cdot$allyl are essentially the same as those of $MoOCl_2(NH)\cdot\cdot$allyl and of $MoOCl_2O\cdot\cdot$allyl, respectively, they were not presented in detail.

5.3. N-Insertion. After an allyl group adsorbed on an imido group, three more hydrogens should be removed from the complex ($MoOCl_2NH\cdot\cdot CH_2CHCH_2$) before the final product, acrylonitrile (CH_2CHCN), is produced and desorbs, leaving behind the reduced molybdenum site, $MoOCl_2$.

5.3.1. 2nd Hydrogen Abstraction: Abstraction from the $C_\alpha-H_\alpha$ bond. We calculated the bond strengths of two weakest bonds ($C_\alpha-H_\alpha$ and N−H bonds) in $MoOCl_2NH\cdot\cdot CH_2CHCH_2$ (**12a**) (Table 13). On the basis of the values shown in Table 6, the other two bonds ($C_\beta-H_\beta$ and $C_\gamma-H_\gamma$ bonds) are expected to be much stronger than these. The $C_\alpha-H_\alpha$ bond strength seems to be similar on imido groups of $MoO(NH)Cl_2$ and of $Mo(NH)_2OCl_2$, (ΔG_{673} = 40.7 and 39.8 kcal/mol, respectively), and it is weaker than on an oxo group of MoO_2Cl_2 (ΔG_{673} = 48.1 kcal/mol; Table 6).

Several possible reaction pathways were investigated for the second hydrogen abstraction from the $C_\alpha-H_\alpha$ bond of the adsorbed allyl group (Schemes and Tables 14 and 15). Like in oxidation, the hydrogen abstraction by an adjacent molybdenum site (Schemes and Tables 14a, 14b, and 15a) was found to be

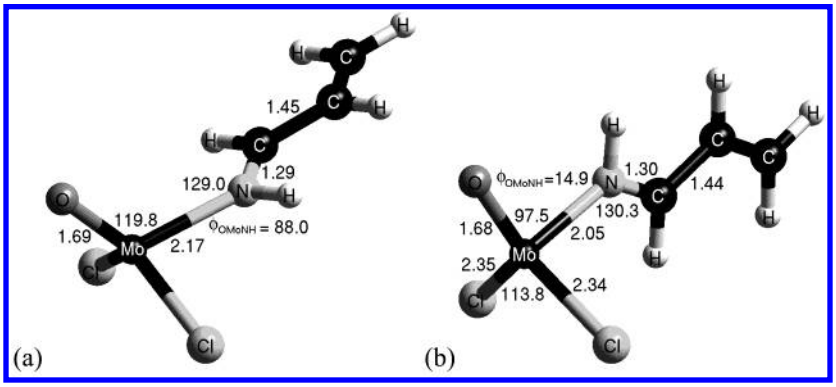

Figure 13. Optimized structures of (a) $^3MoOCl_2\cdot\cdot NHCHCHCH_2$ (**13a**) and (b) $^1MoOCl_2\cdot\cdot NHCHCHCH_2$ (**13a**) resulted from the H removal from the $C_\alpha-H_\alpha$ bond of **12a**. Selected geometrical parameters (bond lengths, angles, and the O−Mo−N−H torsion angle) are shown together in Å and in degrees.

SCHEME 15: Several Possible Pathways of the Second H Abstraction in the Course of Ammoxidation on the "Imido-Imido" Site

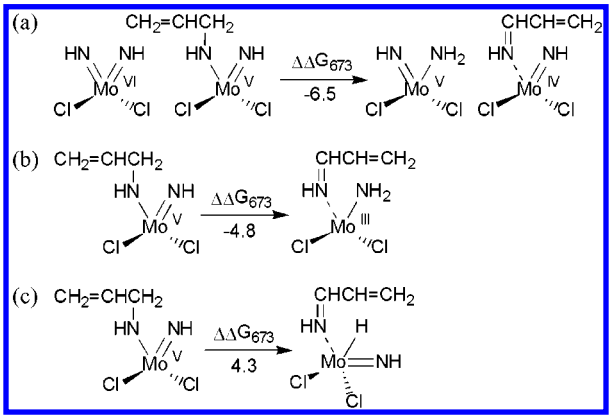

the most favorable (ΔG_{673} = −9.2, −0.5, and −6.5 kcal/mol, respectively). It is more favorable if there is an imido group rather than oxo group as a hydrogen acceptor nearby (Scheme 14a). Thus, it seems that the "oxo-imido" sites next to each other (**9** in Scheme 12) is the best not only in the allyl-adsorbing ability but also in the hydrogen-abstracting ability. Thus, we propose that the best site for ammoxidation is the "oxo-imido" species, as suggested by Allison and Goddard.[7] The second H abstractions from the C_α-H_α bond of **12a**, **12b**, and **12c** by an adjacent site lead to essentially the same conformation of compound $^3MoOCl_2$··$NHCHCHCH_2$ shown in Figure 13a. The optimized structure of $^1MoOCl_2$··$NHCHCHCH_2$ was also shown in Figure 13b for comparison.

5.3.2. 3rd Hydrogen Abstraction: Abstraction from the N−H Bond. In $^3MoOCl_2$··$NHCHCHCH_2$ (**13a**, Figure 13a), the Mo−N bond distance became significantly longer (2.17 Å) than before the H abstraction (1.92 Å), and the $^1CH_2$═CHCH═NH molecular is planar. The energy cost to desorb this premature side product is only 3.6 kcal/mol (Scheme and Table 16a), but this process is still endothermic. This might desorb at this stage and diffuse around on the surface until it finds another reaction site. Or it can go through the third H abstraction, which is exothermic (ΔG_{673} = −5.7 and −4.0 kcal/mol, respectively) if the hydrogen is abstracted from the N−H bond by another oxo-imido site or the oxo-imido group which was already used in the second H abstraction (Scheme and Table 16b and 16d). The optimized structures of $^2MoOCl_2$··$NCHCHCH_2$ and $^4MoOCl_2$··$NCHCHCH_2$ are shown in Figure 14.

5.3.3. 4th Hydrogen Abstraction: Abstraction from the C_α-H_α bond. After the third H abstraction, it does not seem plausible that the $^2CH_2$═CHCH═N· radical could desorb from $^2MoOCl_2$··$NCHCHCH_2$ (**14a**, Figure 14a). The energy cost is as much as 30.2 kcal/mol (Scheme and Table 17). Instead, we expect that the fourth hydrogen abstraction would occur. The energy cost of the hydrogen abstraction from the C_α−H_α bond is only −4.6 kcal/mol if it can find another oxo-imido site present nearby (Scheme 17). The optimized structures of $^3MoOCl_2$··$NCCHCH_2$ and $^1MoOCl_2$··$NCCHCH_2$ are shown in Figure 15.

TABLE 16: Energy Change (kcal/mol) during (a) Desorption of NH═CHCH═CH_2 and (b−c) Third Hydrogen Abstraction from the N−H Bond of $^3MoOCl_2$··$NHCHCHCH_2$ (13a)

	ΔE	ΔZPE	$\Delta\Delta G_{0\rightarrow 673}$	ΔG_{673}
(a) $^3MoOCl_2$··$NHCHCHCH_2$ → $^3MoOCl_2$ + $^1CH_2CHCHNH$	31.7	−1.8	−26.3	3.6
(b) $^3MoOCl_2$··$NHCHCHCH_2$ + $^1MoO(NH)Cl_2$ → $^2MoOCl_2$··$NCHCHCH_2$ + $^2MoO(NH_2)Cl_2$	−3.9	0.2	−1.0	**−5.7**
(c) $^3MoOCl_2$··$NHCHCHCH_2$ + $^1MoO(NH_2)Cl_2$ → $^2MoOCl_2$··$NCHCHCH_2$ + $^2Mo(OH)(NH_2)Cl_2$	−3.9	0.2	−1.0	7.8
(d) $^3MoOCl_2$··$NHCHCHCH_2$ + $^1MoO(NH_2)Cl_2$ → $^2MoOCl_2$··$NCHCHCH_2$ + $^{\|2}MoOCl_2$··NH_3	10.9	−1.9	−1.3	−4.0

SCHEME 16: Several Possible Reaction Pathways from $^3MoOCl_2$··$NHCHCHCH_2$

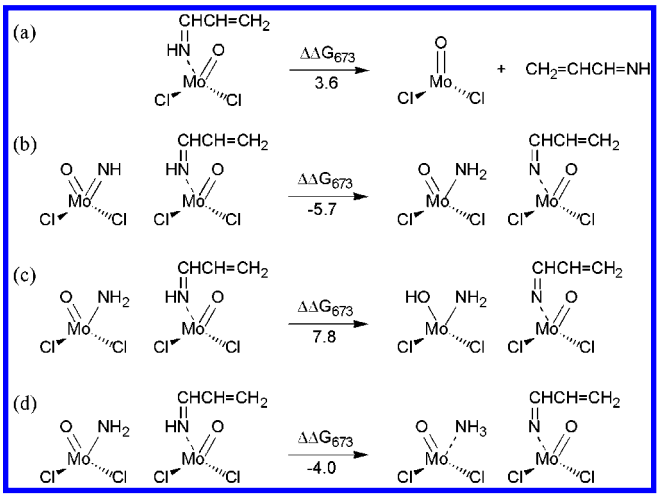

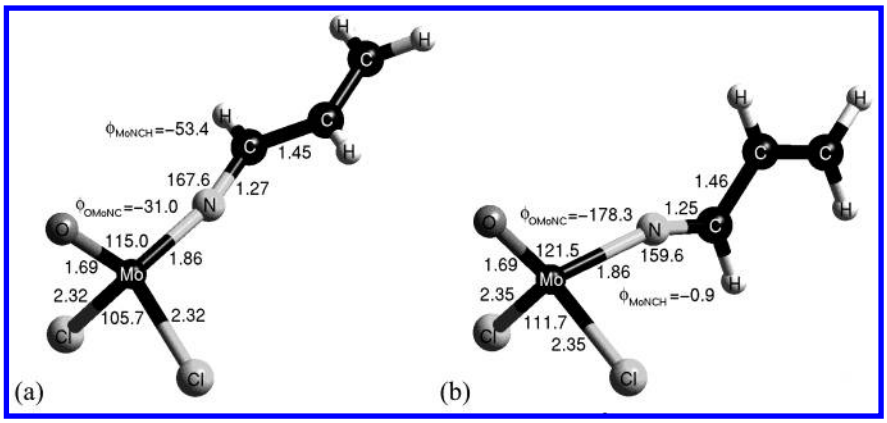

Figure 14. Optimized structures of (a) $^2MoOCl_2$··$NCHCHCH_2$ (**14a**) and (b) $^4MoOCl_2$··$NCHCHCH_2$ (**14b**) resulted from the H removal from the N−H bond of **13a**. Selected geometrical parameters (bond lengths, angles, and torsion angles) are shown together in Å and in degrees.

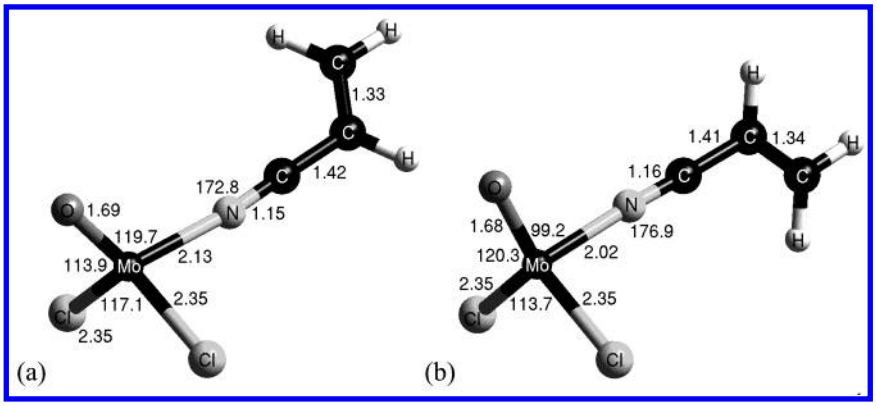

Figure 15. Optimized structures of (a) $^3MoOCl_2\cdot\cdot NCCHCH_2$ (**15a**) and (b) $^1MoOCl_2\cdot\cdot NCCHCH_2$ (**15b**) resulted from the H removal from the N−H bond of **14a**. Selected geometrical parameters (bond lengths, angles, and torsion angles) are shown together in Å and in degrees.

5.3.4. Desorption of Acrylonitrile. Desorption of $^1CH_2{=}CHC{\equiv}N$ from $^3MoOCl_2\cdot\cdot NCCHCH_2$ (**15a**, Figure 15a) leaving behind $^3MoOCl_2$ is exothermic at the reaction temperature (ΔG_{673} = −5.3 kcal/mol, Table 18). This is the desired final product,

SCHEME 17: Several Possible Reaction Pathways from $^3MoOCl_2\cdot\cdot NCHCHCH_2$

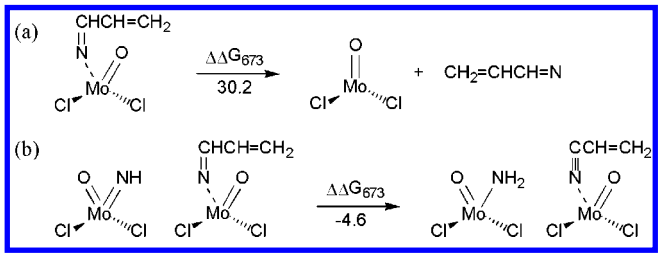

SCHEME 18: Several Possible Reaction Pathways from $^3MoOCl_2\cdot\cdot NCCHCH_2$

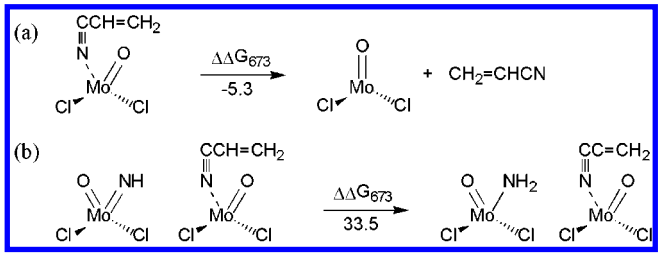

TABLE 17: Energy Change (kcal/mol) during (a) Desorption of $^2CH_2{=}CHCH{=}N\bullet$ and (b−c) Fourth Hydrogen Abstraction from $^2MoOCl_2\cdot\cdot NCHCHCH_2$ (14a)

	ΔE	ΔZPE	$\Delta\Delta G_{0\to673}$	ΔG_{673}
(a) $^2MoOCl_2\cdot\cdot NCHCHCH_2 \rightarrow$ $^3MoOCl_2 + {}^2CH_2CHCHN$	60.1	−2.4	−27.4	30.2
(b) $^2MoOCl_2\cdot\cdot NCHCHCH_2 +$ $MoO(NH)Cl_2 \rightarrow$ $^3MoOCl_2\cdot\cdot NCCHCH_2 +$ $^2MoO(NH_2)Cl_2$	−0.2	−0.1	−4.2	**−4.6**
(c) $^2MoOCl_2\cdot\cdot NCHCHCH_2 +$ $MoO(NH)Cl_2 \rightarrow$ $^1MoOCl_2\cdot\cdot NCCHCH_2 +$ $^2MoO(NH_2)Cl_2$	0.2	−0.1	−1.9	−1.8

TABLE 18: Energy Change (kcal/mol) during (a) Desorption of Acrylonitrile and (b−c) the Fifth Hydrogen Abstraction from $^3MoOCl_2\cdot\cdot NCCHCH_2$ (15a)

	ΔE	ΔZPE	$\Delta\Delta G_{0\to673}$	ΔG_{673}
(a) $^3MoOCl_2\cdot\cdot NCCHCH_2 \rightarrow$ $^3MoOCl_2 + {}^1CH_2{=}CHCN$	20.6	−1.2	−24.7	**−5.3**
(b) $^3MoOCl_2\cdot\cdot NCCHCH_2$ $+ MoO(NH)Cl_2 \rightarrow$ $^2MoOCl_2\cdot\cdot NCCCH_2 +$ $^2MoO(NH_2)Cl_2$	29.4	3.7	7.2	40.3
(c) $^2MoOCl_2\cdot\cdot NCCHCH_2 +$ $MoO(NH)Cl_2 \rightarrow$ $^4MoOCl_2\cdot\cdot NCCCH_2 +$ $^2MoO(NH_2)Cl_2$	39.9	−2.6	−4.1	33.5

SCHEME 19: Ammoxidation

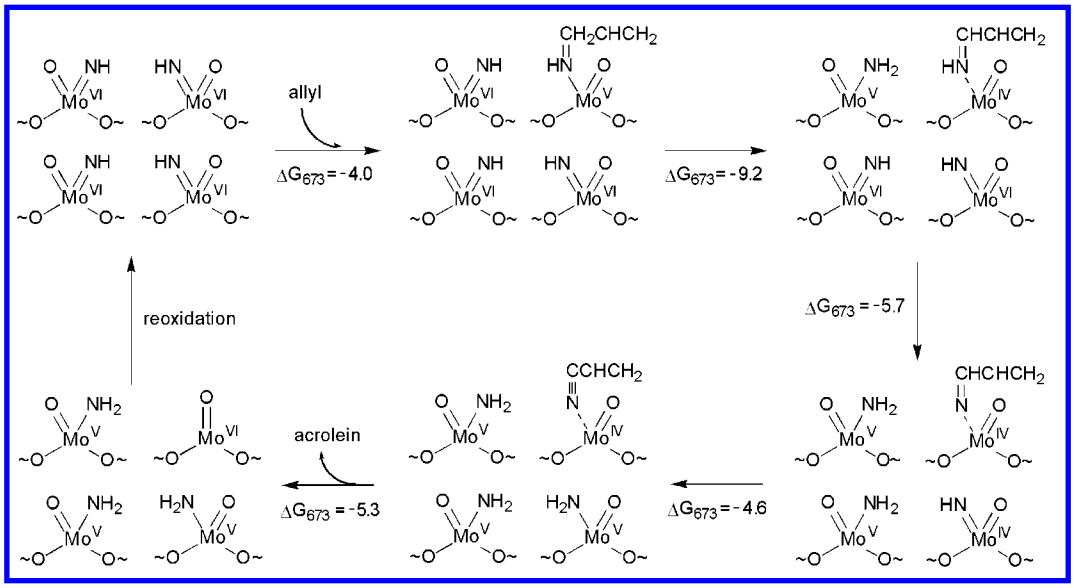

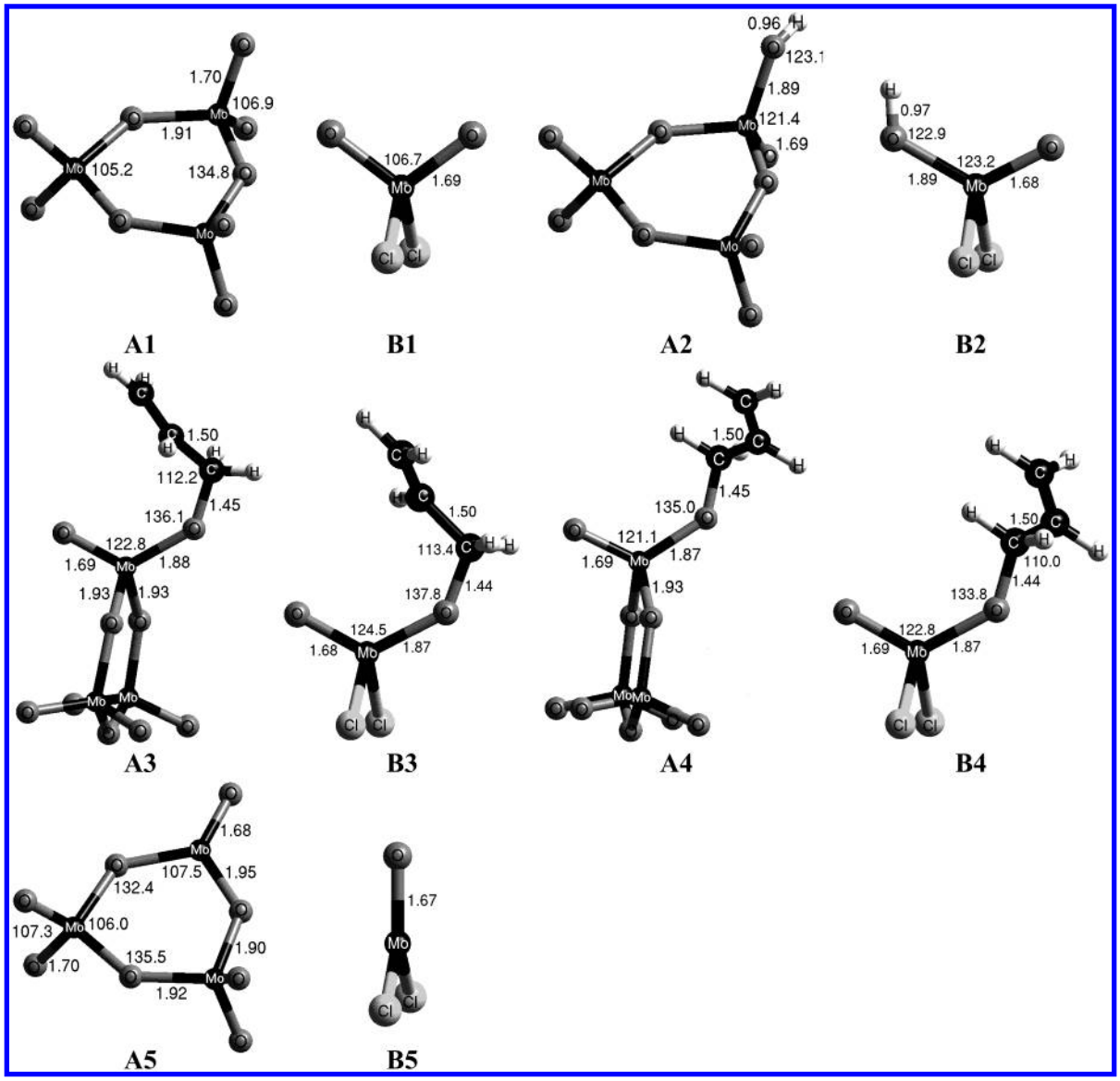

Figure A. Mo_3O_9 versus MoO_2Cl_2.

TABLE A: Mo_3O_9 versus MoO_2Cl_2

(a) H adsorption on the oxo oxygen	ΔE	ΔZPE	$\Delta\Delta G_{0\rightarrow 673}$	ΔG_{673}
Mo_3O_9 (**A1**) + propene → Mo_3O_9_H (**A2**) + allyl	32.9	−2.4	−3.4	27.1
MoO_2Cl_2 (**B1**) + propene → MoO_2Cl_2_H (**B2**) + allyl	34.4	−2.1	−2.5	29.8
(b) Allyl adsorption (two conformations)	ΔE	ΔZPE	$\Delta\Delta G_{0\rightarrow 673}$	ΔG_{673}
Mo_3O_9 (**A1**) + allyl → Mo_3O_9_allyl (**A3**)	−21.3	?	?	?
MoO_2Cl_2 (**B1**) + allyl → MoO_2Cl_2_allyl (**B3**)	−20.5	3.6	23.6	6.7
Mo_3O_9 (**A1**) + allyl → Mo_3O_9_allyl (**A4**)	−21.4	?	?	?
MoO_2Cl_2 (**B1**) + allyl → MoO_2Cl_2_allyl (**B4**)	−20.3	3.6	23.2	6.5
(c) reoxidation	ΔE	ΔZPE	$\Delta\Delta G_{0\rightarrow 673}$	ΔG_{673}
Mo_3O_8 (**A5**) + $0.5O_2$ → Mo_3O_9 (**A1**)	−72.9	1.5	15.3	−56.1
$MoOCl_2$ (**B5**) + $0.5O_2$ → MoO_2Cl_2 (**B1**)	−68.5	1.3	14.4	−52.8

acrylonitrile. On the other hand, the fifth hydrogen abstraction from the $C_\beta-H_\beta$ or $C_\gamma-H_\gamma$ bonds are very endothermic (ΔG_{673} > 30 kcal/mol). Thus, acetonitrile is expected to be desorbed exclusively at this stage.

5.4. Summary: Ammoxidation. Our calculation indicated that ammonia activation would be easier on Mo(IV) rather than on Mo(VI). Ammonia would be activated more easily for more reducing condition. Because ammonia and propene are reducing agents, higher partial pressures of them could accelerate the ammonia activation. This is consistent with the kinetic model of ammoxidation proposed by Grasselli and co-workers that imido sites (Mo═NH) are more abundant in higher partial pressures of feed.

Our calculations also indicate that allyl groups produced as a result of the hydrogen abstraction from propenes would be adsorbed more easily on imido groups (Mo═NH) than on oxo

groups (Mo═O) and that the spectator oxo effect is larger than spectator imido effect. Thus, the best site for the allyl adsorption is the imido group of the "oxo-imido" species. This site was also the best in the hydrogen abstraction from the adsorbed allyl group. Thus, we propose that the best site for ammoxidation is the "oxo-imido" species.

On the basis of the energetics, we speculate that four such sites are required for the most favorable ammoxidation, but three sites or even two sites are also likely to do the same job without losing much efficiency. The overall reaction scheme is summarized in Scheme 19.

Acknowledgment. We thank Asahi Chemical Ind. Co., Ltd., Fuji, Shizuoka 416-8501, Japan for providing funding for this project and Dr. Terumasa Yamasaki of Asahi Chemical for helpful comments. Some support was provided by the ARO/MURI (DAAD 19-01-1-0517). We also thank Dr. Bob Grasselli and Dr. Jim Burrington for many helpful discussions over the years. The facilities of the MSC are also supported by grants from NSF-MRI, DOE-ASCI, ARO/MURI, Chevron, 3M, Beckman Institute, Seiko-Epson, Dow, Avery-Dennison, Kellogg, NSF-CHE, NIH, and ARO/DURIP.

Appendix A. Mo_3O_9 versus MoO_2Cl_2

In section 3.1, we found that the terminal oxo oxygens (═O) in Mo_3O_9 are much more active than the bridging oxygens (−O−). This suggests that the reactions can be described by including only oxo oxygens in the model (no bridging oxygens). Thus, to simplify and reduce the costs of the calculations, we replaced the bridging oxygens with chlorines, that is, replaced Mo_3O_9 (**A1**) with MoO_2Cl_2 (**B1**). To determine the effect of this replacement, we calculated the energy changes involved in several key reactions on these two model clusters: (1) H adsorption, (2) allyl adsorption in two different conformation, and (3) reoxidation from Mo(IV) to Mo(VI) (Figure and Table A). The energy changes calculated using the simple MoO_2Cl_2 model are quite similar to those calculated on the more complicated Mo_3O_9 model. This validates the use of the simple MoO_2Cl_2 model.

Note Added after ASAP Posting. This article was released ASAP on 5/18/2002 without the author's corrections to the last five pages. The correct version was posted on 5/23/2002.

References and Notes

(1) Hearne, G. W.; Adams, M.; Shell Development Co.: U. S. Patent 2, 1948; Vol. 451, pp 485.
(2) Idol, J. D.; Standard Oil, Co., Ohio (SOHIO): U. S. Patent 2, 1959; Vol. 904, pp 580.
(3) Moro-Oka, Y.; Ueda, W. *Adv. Catal.* **1994**, *40*, 233.
(4) Grasselli, B. K.; Burrington, J. D.; Brazdil, J. F. *Faraday Discussions* **1981**, *72*, 203.
(5) Habor, J.; Grzybowska, B. *J. Catal.* **1973**, *28*, 489.
(6) Grasselli, R. K.; Burrington, J. D.; Brazdil, J. F. *Faraday Diss.* **1981**, *72*, 203.
(7) Allison, J. N.; Goddard, W. A. I. *Active Sites on Molybdenum Surfaces, Mechanistic Considerations for Selective Oxidation and Ammoxidation of Propene*; Grasselli, R. K., Bradzil, J. F., Ed.; American Chemical Society: Washington, DC, 1985; Vol. 279, pp 23.
(8) Kihlborg, L. *Arkiv Kemi.* **1963**, *21*, 357.
(9) Harwig, H. A. *Anorg. Allg. Chem.* **1978**, *444*, 151.
(10) van den Elzen, A. F.; Rieck, G. D. *Acta Cryst. B* **1973**, *29*, 2433.
(11) Theobald, F.; Laarif, A. *Mater. Res. Bull.* **1985**, *20*, 653.
(12) Berkowitz, J.; Inghram, M. G.; Chupka, W. A. *J. Chem. Phys.* **1957**, *26*, 842.
(13) Maleknia, S.; Brodbelt, J.; Pope, K. *J. Am. Soc. Mass Spect.* **1991**, *2*, 212.
(14) Fialko, E. F.; Kikhtenko, A. V.; Goncharov, V. B.; Zamazaev, K. I. *J. Phys. Chem. A* **1997**, *101*, 8607.
(15) France, M. R.; Buchanan, J. W.; Robinson, J. C.; Pullins, S. H.; Tucker, J. L.; King, R. B.; Duncan, M. A. *J. Phys. Chem. A* **1997**, *101*, 6214.
(16) Sidorov, L. N.; Minayeva, I. I.; Zasorin, E. Z.; Sorokin, I. D.; Borshchevskiy, A. Y. *High Temp. Sci.* **1980**, *12*, 175.
(17) Bienati, M.; Bonacic-Koutecky, V.; Fantucci, P. *J. Phys. Chem. A* **2000**, *104*, 6983.
(18) Oniyama, E.; Wahlbeck, P. G. *J. Phys. Chem. B* **1998**, *102*, 4418.
(19) Fielicke, A.; Rademann, K. *J. Phys. Chem. A* **2000**, *104*, 6979.
(20) Kinne, M.; Heidenreich, A.; Rademann, K. *Angew. Chem., Int. Ed. Engl.* **1998**, *37*, 2509.
(21) Kinne, M.; Rademann, K. *Chem. Phys. Lett.* **1998**, *284*, 363.
(22) Slater, J. C. *Quantum Theory of Molecules and Solids. Vol. 4. The Self-Consistent Field for Molecules and Solids*; McGraw-Hill: New York, 1974.
(23) Becke, A. D. *Phys. Rev. A* **1988**, *38*, 3098.
(24) Vosko, S. H.; Wilk, L.; Nusair, M. *Can. J. Phys.* **1980**, *58*, 1200.
(25) Lee, C. T.; Yang, W. T.; Parr, R. G. *Phys. Rev. B* **1988**, *37*, 785.
(26) Miehlich, B.; Savin, A.; Stoll, H.; Preuss, H. *Chem. Phys. Lett.* **1989**, *157*, 200.
(27) Dunning, T. H., Jr. *J. Chem. Phys.* **1989**, *90*, 1007.
(28) Kendall, R. A.; Dunning Jr., T. H.; Harrison, R. J. *J. Chem. Phys.* **1992**, *96*, 6796.
(29) Hay, P. J.; Wadt, W. R. *J. Chem. Phys.* **1985**, *82*, 299.
(30) *Jaguar 3.5*; Schrodinger Inc.: Portland, OR, 1998.
(31) Greeley, B. H.; Russo, T. V.; Mainz, D. T.; Friesner, R. A.; Langlois, J.-M.; Goddard, W. A., III; Donnelly, R. E.; Ringalda, M. N. *J. Chem. Phys.* **1994**, *101*, 4028.
(32) *CRC Handbook of Chemistry and Physics, 80th Ed.*; CRC Press: Boca Raton, 1999−2000.
(33) Berkowitz, J.; Ellison, G. B.; Gutman, D. *J. Phys. Chem.* **1994**, *98*, 2744.
(34) Ellison, G. B.; Davico, G. E.; Bierbaum, V. M.; DePuy, C. H. *Int. J. Mass Spectrom. Ion Proc.* **1997**, *156*, 109.
(35) Pedley, J. B.; Marshall, E. M. *J. Phys. Chem. Ref. Data* **1984**, *12*, 967.
(36) Uy, O. M.; Drowart, J. *Trans. Faraday Sco.* **1969**, *65*, 3221.
(37) Loock, H.-P.; Simard, B.; Wallin, S.; Linton, C. *J. Chem. Phys.* **1998**, *109*, 8980.
(38) Chen, M.; Waghmare, U. V.; Friend, C. M.; Kaxiras, E. *J. Chem. Phys.* **1998**, *109*, 6854.
(39) Hermann, K.; Witko, M.; Michalak, A. *Catal. Today* **1999**, *50*, 567.
(40) Rappe, A. K.; W. A. Goddard, I. *J. Am. Chem. Soc.* **1982**, *104*, 3287.
(41) Glaeser, L. C.; Brazdil, J. F.; Hazle, M. A.; Mehicic, M.; Grasselli, R. K. *J. Chem. Soc. Faraday Trans. I* **1985**, *81*, 2903.
(42) Grasselli, R. K. *J. Chem. Educ.* **1986**, *63*, 216.
(43) Mizoguchi, H.; Kawazoe, H.; Hosona, H.; Fujitsu, S. *Solid State Commun.* **1997**, *104*, 705.
(44) Mizoguchi, H.; Ueda, K.; Kawazoe, H.; Hosono, H.; Omata, T.; Fujitsu, S. *J. Mater. Chem.* **1997**, *7*, 943.
(45) Grasselli, R. K.; Callahan, J. L. *J. Catal.* **1969**, *14*, 93.
(46) Grasselli, R. K.; Suresh, D. D. *J. Catal.* **1972**, *25*, 273.
(47) Swift, H. E.; Bozik, J. E.; Ondrey, J. A. *J. Catal.* **1971**, *21*, 212.
(48) Grasselli, R. K. *Appl. Catal.* **1985**, *15*, 127.
(49) Burrington, J. D.; Kartisek, C. T.; Grasselli, R. K. *J. Catal.* **1984**, *87*, 363.
(50) Jang, Y. H.; Goddard, W. A., III *Top. Catal.* **2001**, *15*, 273.